Title: **FRINGE OR BACKGROUND: CHARACTERIZING DEEP-WATER MUDSTONES BEYOND THE BASIN-FLOOR FAN SANDSTONE PINCHOUT**

Authors: KÉVIN BOULESTEIX[1*], MIQUEL POYATOS-MORÉ[2], DAVID M. HODGSON[3], STEPHEN S. FLINT[1], KEVIN G. TAYLOR[1]

Institutions:

[1]Department of Earth and Environmental Sciences, University of Manchester, Oxford Road, Manchester M13 9PL, UK

[2]Department of Geosciences, University of Oslo, Oslo 0371, Norway

[3]School of Earth and Environment, University of Leeds, Leeds LS2 9JT, UK

*Email: kevin.boulesteix@gmail.com

Keywords: Deep-water, basin-floor, mudstone, processes, architecture, Karoo Basin

ABSTRACT

Mud dominates volumetrically the fraction of sediment delivered and deposited in deep-water environments, and mudstone is a major component of basin-floor successions. However, studies of basin-floor deposits have mainly focused on their proximal sandstone-prone part. A consequent bias therefore remains in the understanding of depositional processes and stratigraphic architecture in mudstone-prone distal settings beyond the sandstone pinchouts of basin-floor fans. This study uses macroscopic and microscopic descriptions of over 500 m of continuous cores from research boreholes from the Permian Skoorsteenberg Formation of the Karoo Basin, South Africa, to document the sedimentology, stratigraphy and ichnology of a distal mudstone-prone basin-floor succession. Very thin- to thin-bedded mudstones, deposited by low-density turbidity currents, stack to form bedsets bounded by thin packages (<0.7 m thick) of background mudstones. Genetically-related bedsets stack to form bedset packages, which are bounded by thicker (>0.7 m thick) background mudstones. Stratigraphic correlation between cores suggests that bedsets represent the distal fringes of submarine fan lobe elements and/or lobes, and bedset packages represent the distal fringes of lobe complexes and/or lobe complex sets. The internal stacking pattern of bedsets and bedset packages is highly variable vertically and laterally, which records dominantly autogenic processes (e.g. compensational stacking, avulsion of feeder channels). The background mudstones are characterized by remnant tractional structures and outsize particles, and are interpreted as deposited from low-density turbidity currents and debris flows prior to intense biogenic reworking. These observations challenge the idea that mud only accumulate from hemipelagic suspension fallout in distal basin-floor environments. Thin background mudstones separating bedsets (<0.7 m thick) are interpreted to mainly represent autogenically-driven lobe abandonment due to up-dip channel avulsion. The thicker background mudstones separating bedset packages (>0.7 m thick) are interpreted to dominantly mark allogenically-driven regional decrease of sand supply to the basin-floor. The recognition of sandstone-prone basin-floor fans passing into genetically-linked distal fringe mudstones suggests that submarine lobes are at least ~20 km longer than previously estimated. This study provides sedimentological, stratigraphic and ichnological criteria to differentiate mudstones deposited in different sub-environments within distal deep-water basin-floor

settings, with implications for the accurate characterization of basin-floor fan architecture, and their use as archives of paleoenvironmental change.

INTRODUCTION

Basin-floor fans are amongst the largest sediment accumulations on Earth (e.g. Normark 1970; Mutti 1977; Hodgson et al. 2006; Deptuck et al. 2008; Grundvåg et al. 2014; Picot et al. 2016; Pickering et al. 2020). The building blocks of basin-floor fans are lobes, which can be subdivided from proximal to distal environments into lobe axis, off-axis, fringe and distal fringe (Fig. 1) (Prélat et al. 2009). The mudstone/sandstone ratio increases from lobe axis to fringe, and the transition from lobe fringe to distal fringe is commonly marked by the position of the sandstone pinchout (Fig. 1) (Prélat et al. 2009; Spychala et al. 2017; Hansen et al. 2019). Basin-floor fans are a component of basin-floor environments. However, mud-prone deposits beyond submarine fans are typically treated as unrelated, or referred to as background deposits (Fig. 1) (e.g. Grundvåg et al. 2014; Spychala et al. 2017; Pierce et al. 2018). Mud—here defined as <62.5 µm particles (i.e. clay- and silt-size particles; *sensu* Lazar et al. (2015))––dominates the fraction of sediment delivered by rivers to modern oceans (Burgess and Hovius 1998), and mudstone (sedimentary rock with more than fifty percent of mud-size particles) is consequently a major component of deep-water successions. However, sedimentological and stratigraphic studies of basin-floor deposits have mainly focused on proximal sandstone-prone basin-floor fan successions (i.e. lobe axis to fringe) (e.g. Satur et al. 2000; Johnson et al. 2001; Hodgson et al. 2006; Etienne et al. 2012; Grundvåg et al. 2014; Terlaky et al. 2016; Spychala et al. 2017). This results in less developed understanding of depositional processes and stratigraphic architecture in distal mudstone-prone basin-floor deposits (i.e. lobe distal fringe, basin-floor background), beyond the sandstone pinchout of basin-floor fans.

A combination of allogenic (e.g. eustasy, climate, tectonics) and autogenic (e.g. channel avulsion, compensational stacking) processes control the architecture of basin-floor fans (e.g. Johnson et al. 2001; Hodgson et al. 2006; Prélat et al. 2009; Grundvåg et al. 2014; Blum et al. 2018; Burgess et al. 2019;

Sweet et al. 2019; Ferguson et al. 2020). A longstanding consideration in the assessment of basin-floor fan successions relates to the interpretation of mudstone packages intercalated between lobe axis to fringe deposits. These fine-grained basin-floor deposits have been commonly interpreted as regional background deposits that drape basin-floor fans, indicating an allogenically-driven decrease in sand supply to the basin-floor during relative sea-level rise, with sand trapped on the coeval shelf or slope (e.g. Satur et al. 2000; Johnson et al. 2001; Hodgson et al. 2006; Flint et al. 2011). Alternatively, some mudstone packages have been interpreted as the genetically-linked distal fringes of basin-floor fans, formed by autogenic processes, while sand was deposited elsewhere on the basin-floor (e.g. Prélat and Hodgson 2013; Spychala et al. 2017). An accurate distinction between these two interpretations requires the regional mapping of mudstone packages to test whether they grade to sandstones in a lateral and/or up-dip positions (autogenic interpretation), or if they are laterally continuous across the basin-floor (allogenic interpretation) (Prélat and Hodgson 2013). Differentiating mud transported and deposited by processes related to lobe distal fringe environments from basin-floor background mud, not genetically linked to any lobe, has major implications for the dimensions of basin-floor fans, and for the correct interpretation of depositional rates and sediment mass balance in deep-water environments (e.g. Hesse 1975). This may also aid the stratigraphic prediction of deep-water sandstone hydrocarbon reservoirs along basin margins. The distal fringe environments of basin-floor fans are also preferential sites of organic matter deposition and can form source rocks (Huc et al. 2001; Mignard et al. 2017), host unconventional hydrocarbon accumulations, or act as effective seals. Anthropogenic pollutants can also reach distal basin-floor environments through transport and deposition by sediment gravity flows (Kane and Clare 2019; Pohl et al. 2020). Therefore, sedimentological and stratigraphic characterization of distal basin-floor deposits may also help to predict the extent and volume of a wide range of particles in modern basin-floor environments. Distal basin-floor successions have been also used for the study of sea-level and paleoclimatic changes (e.g. Schmitz et al. 2001; Payros et al. 2012; Bornemann et al. 2014; Cantalejo and Pickering 2014; Payros and Martínez-Braceras 2014), since they can offer a more continuous record with greater preservation of individual depositional events compared to proximal sandstone-prone basin-floor deposits.

This study aims to use a subsurface dataset from research boreholes set in the well-constrained regional stratigraphic context of the Permian Skoorsteenberg Formation, in the Tanqua Karoo (South Africa). We present for the first time a multi-scale sedimentological, stratigraphic, and ichnological investigation of a thick deep-water mudstone-prone distal basin-floor succession. Specific objectives are to: 1) characterize the range of facies, transport and depositional processes, trace fossils, and stacking patterns in distal basin-floor deposits; 2) discuss sedimentological, stratigraphic, and ichnological criteria to distinguish lobe distal fringe mudstones from basin-floor background mudstones; 3) constrain the dimensions of deep-water lobes including their distal fringe deposits; and 4) refine depositional models of deep-water lobes including the distal fringe and basin-floor background deposits.

GEOLOGICAL SETTING

The Karoo Basin has been interpreted as a retroarc foreland basin that formed during the Carboniferous and Permian on the southern margin of Gondwana, with subsidence controlled by flexural loading linked to the development of a magmatic arc and associated fold-thrust belt (Cape Fold Belt) (De Wit and Ransome 1992; Veevers et al. 1994; Visser and Praekelt 1996; Catuneanu et al. 1998; López-Gamundí and Rossello 1998; Viglietti et al. 2017). Other studies have suggested that subsidence during the Carboniferous and Permian was caused by dynamic topography (mantle flow), linked to the subduction of the paleo-Pacific plate beneath Gondwana (Pysklywec and Mitrovica 1999; Tankard et al. 2009; 2012). In the latter model, flexural subsidence linked to loading from the development of the Cape Fold Belt occurred later, during the Triassic (Tankard et al. 2009, 2012; Blewett and Phillips 2016).

Located in the south-western corner of the Karoo Basin, the Tanqua depocenter is bounded to the south by the Swartberg Branch and to the west by the Cederberg Branch of the Cape Fold Belt (Fig. 2A). The sedimentary fill is part of the Karoo Supergroup, subdivided into the glaciogenic Dwyka Group (Late Carboniferous to Early Permian), the post-glacial clastic marine Ecca Group (Early Permian to Middle

Permian), and the continental fluvial Beaufort Group (Middle Permian to Early Triassic) (Fig. 2B; Smith 1990; Johnson et al. 1996; Catuneanu et al. 2005). The lower Ecca Group (Prince Albert, Whitehill, Collingham and Tierberg formations) consists of an approximately 600 m-thick mudstone-prone basin-floor succession, dominated by sediment-gravity flow deposits, associated with minor slumps and slides (Fig. 2B) (Visser 1992; Viljoen 1994; Chukwuma and Bordy 2016; Boulesteix et al. 2019). The overlying 450 m-thick upper Ecca Group consists of basin-floor fans of the Skoorsteenberg Formation (Bouma and Wickens 1994; Wickens 1994; Morris et al. 2000; Johnson et al. 2001; Hodgson et al. 2006) overlain by the 300 m-thick upper slope to shelf-deltaic deposits of the Waterford Formation (Wild et al. 2009; Dixon et al. 2012; Gomis-Cartesio et al. 2016; Poyatos-Moré et al. 2016).

The Skoorsteenberg Formation is characterized by a narrow grain size range (mud to fine sand), and consists of four basin-floor fans (Fans 1-4; Bouma and Wickens 1994), and an overlying base-of-slope to slope succession (Unit 5; Wickens 1994; Wild et al. 2009). Integration of regional field mapping and sedimentary logging, supplemented by the description and interpretation of 2140 m of continuous cores from eleven research boreholes, has constrained the sedimentology and stratigraphic architecture of Fans 1-4 (Fig. 3A) (Hodgson et al. 2006; Luthi et al. 2006; Prélat et al. 2009; Spychala et al. 2017; Hansen et al. 2019). Paleocurrent indicators are dominantly to the north/northeast, and the fans are interpreted to be mainly point-sourced from the southwest (Fig. 3B) (Johnson et al. 2001; Hodgson et al. 2006). Fans 1-4 are each up to 65 m thick, and are separated vertically by regionally extensive mudstones (Wickens 1994; Johnson et al. 2001; Hodgson et al. 2006). Each fan is characterized by a progradational-aggradational-retrogradational stacking pattern of constituent lobes (Johnson et al. 2001; Hodgson et al. 2006). In a sequence stratigraphic framework, Fans 1-4 are each interpreted as a lowstand systems tract, with each overlying regionally extensive mudstone interpreted as the combined transgressive and highstand systems tracts (Flint et al. 2011).

This study focuses on the mudstone-prone basin-floor deposits situated in a distal/lateral position relative to the sandstone-prone sections of Fans 1, 2 and 3 (Fig. 3A). Fan 1 is the least well exposed of the four fans, cropping out only in the westernmost part of the Tanqua depocenter (Fig. 3B). Here, Fan 1 has a maximum thickness of 20 m, and approximately 15 m of regionally extensive mudstone

7

separates Fan 1 from Fan 2 (Hodgson et al. 2006). Fan 2 is also exposed in the western part of the depocenter (Fig. 3B), and has a maximum thickness of 40 m. It consists of three sandstone-prone packages separated by mudstone-prone units. Approximately 35 m of regionally extensive mudstone separates Fan 2 and Fan 3 (Hodgson et al. 2006). A sandstone-prone package is present between Fan 2 and Fan 3 (here referred as Unit 2/3). Fan 1, Fan 2 and Unit 2/3 gradually thin to the northeast (Johnson et al. 2001; Hodgson et al. 2006).

MATERIALS AND METHODS

The subsurface dataset used in this study comprises five continuous cores from research boreholes (OR01, NB2, NB3, NB4 and NS2) (Fig. 3). Facies descriptions and interpretations are mainly based on visual and microscopic core observations from the OR01 borehole, supplemented by visual observations from NB2, NB3, NB4 and NS2 (cumulative thickness of 544 m). Following the guidelines of Lazar et al. (2015), cores were logged graphically through dry and wet observations of well-polished surfaces to record macroscopically visible features including: (i) lithology, (ii) color, (iii) sedimentary structures, (iv) bed contacts, (v) bed thicknesses, (vi) deformation, (vii) trace fossils and (viii) bioturbation index. The core descriptions allowed defining three mudstone facies and six sandstone facies. The terminology from Campbell (1967) was used to describe bed thicknesses, where a very thin bed is up to 3 cm thick, and a thin bed ranges from 3 to 10 cm thick. The descriptive bioturbation index (BI) of Taylor and Goldring (1993) was used on a 0-6 scale to quantify bioturbation intensity, where 0 corresponds to non-bioturbated sediment, and 6 corresponds to completely bioturbated and homogenized sediment. The presence of calcium carbonate was assessed by dropping 5% hydrochloric acid onto the core. Enhanced contrast images of the cores using Microsoft Office Picture Manager® helped to capture subtle color changes, bed contacts and trace fossils.

A total of 63 samples were collected from OR01 using an adjusted uniform sampling spacing method of one sample per 3 m to include all facies and features of interest (i.e. facies contacts, trace fossils, diagenetic features). Of these, 28 samples were selected from different stratigraphic packages to

represent the range of mudstone facies described at core scale, and were prepared for ultra-thin (20-25 µm thick) polished thin sections (24×46 mm) oriented normal to the bedding orientation. Thin sections were scanned using an Epson Perfection V600 photo scanner at 3200 dpi resolution. Microscopic descriptions were performed using an optical Nikon Eclipse LV100NPOL microscope fitted with a Nikon DS-Fi2 camera. The microscopic descriptions focused on the characterization of the millimeter-scale sedimentary features (grading, bed contacts, laminations), grain size, composition, bioturbation and diagenetic features. Mudstones with more than half the grains <10 µm were classified as fine mudstones, and mudstones with more than half the grains >10 µm as coarse mudstones (McCave et al. 1995). A composition modifier (siliceous, calcareous, argillaceous and carbonaceous) was added depending on the dominant grain type (quartz, carbonate, clay and organic matter respectively). Stratigraphic changes in bioturbation index, burrows size, and ichnodiversity were used qualitatively to infer paleo-seafloor physicochemical conditions (oxygen level, sedimentation rate, frequency of flow events) (e.g. Bromley 1996; Gingras et al. 2011).

FACIES, DEPOSITIONAL PROCESSES AND ICHNOLOGY

Nine sedimentary facies (F1-F9) are observed in the succession. Three mudstone facies (F1-F3) are described and interpreted below (Fig. 4). Other illustrations of the mudstone facies are shown in Figures 5 to 9. Six sandstone facies (F4-F9) are summarized in Table 1. The range of ichnotaxa identified in the succession is shown in Figure 10.

Facies 1 (F1): Normally Graded Mudstone

Description.--- Facies 1 (F1) consists of light- to mid-gray, moderately- to well-sorted, siliceous-argillaceous, very thin- to thin-bedded fine to coarse mudstone (Fig. 4A, B). Beds are laterally continuous at core scale, and range in thickness from 0.05 to 4 cm, but are typically <0.5 cm thick (Figs. 4A, 5A). Bed bases are sharp or erosional, and occasionally characterized by flame structures (Fig. 4B). Beds are normally graded, marked by a light- to mid-gray color grading (Figs. 4A, 5A), associated with

an upward increase in clay content (Fig. 5C, D). Some beds are characterized by a tripartite microstratigraphy (Fig. 5C). The lower subdivision (1) consists of normally graded fine to coarse mudstone associated with continuous to discontinuous planar-parallel laminations. The middle subdivision (2) consists of normally graded fine to coarse mudstone. The upper subdivision (3) consists of ungraded mottled fine mudstone. However, most beds are devoid of the lower planar-parallel laminated subdivision (Figs. 4B, 5D). The contacts between the bed subdivisions are usually gradational and bioturbated (Fig. 5C, D). Part of this facies is characterized by a gradual upward decrease in bed dip angle (Fig. 5A). Some sections also exhibit scours and soft-sediment deformation (Fig. 5B). Grains consist of quartz, feldspar and clay, with minor associated organic fragments, zircon and apatite (Fig. 5E). Bioturbation is sparse to low (BI: 1-2), and ichnotaxa consist of *Chondrites*, *Helminthopsis*, *Planolites* and *Phycosiphon*, which are generally <0.5-cm in diameter (Fig. 10).

Interpretation.--- Based on the sharp or erosional base, normal grading, and bioturbated top, individual beds of F1 are interpreted to have been deposited by waning, low-density turbidity currents (*sensu* Lowe 1982). The lower normally graded planar-parallel laminated bed subdivision (1) indicates deposition by suspension fallout with evidence for tractional reworking (Piper 1978; Stow and Shanmugam 1980). The middle normally graded bed subdivision (2) and upper ungraded bed subdivision (3) indicate deposition by suspension fallout from the most dilute part of the turbidity current. The flame structures suggest relatively high sedimentation rates (Stow and Shanmugam 1980). The occasional gradual upward decrease of bed dip angle suggests scour fill at a larger scale than the core width.

Facies 2 (F2): Faintly Bedded Mudstone

Description.--- Facies 2 (F2) consists of light- to mid-gray, moderately- to poorly-sorted, siliceous-argillaceous, faintly very thin- to thin-bedded fine to coarse mudstone (Fig. 4C, D). Beds are usually laterally discontinuous at core scale, and range in thickness from 0.05 to 4 cm, but are typically <0.5 cm thick (Figs. 4C, 4D, 6A). The lower and upper bed contacts are gradational due to bioturbation (Figs. 4D, 6B, 6C, 6D). Beds are usually characterized by a subtle light- to dark-gray color grading, associated

with a very weak normal grading (Figs. 4D, 6D). Grains consist of quartz, feldspar and clay, with minor associated organic fragments, zircon and apatite, similar to F1 (Fig. 6E). Bioturbation is moderate to high (BI: 3–4), and ichnotaxa consists of *Chondrites, Helminthopsis*, *Nereites*, *Planolites* and *Phycosiphon* (Fig. 10). Burrows are usually larger than in F1 (<2-cm in diameter). Pyrite nodules are more common than in F1 (Fig. 6E).

Interpretation.--- Based on the faintly-bedded texture and the weak normal grading, individual beds of F2 are interpreted to have been primarily deposited by waning, low-density turbidity currents (*sensu* Lowe 1982), similar to F1, before being reworked by bioturbation. However, the smaller amount of preserved tractional structures (i.e. laminations), weak normal grading, more common bioturbation, and larger burrow size suggest F2 was deposited from lower energy flows and under lower sedimentation rate compared to F1 (Gingras et al. 2011).

Facies 3 (F3): Mottled Mudstone

Description.--- Facies 3 (F3) consists of light- to dark-gray, argillaceous-siliceous, fine to coarse mudstone characterized by a distinctive mottled texture (Figs. 4E, 4F, 7A, 7B). Some packages are characterized by intercalated mudstones of various colours (from light to dark gray) on a scale of centimeters to decimeters (Fig. 7A). From thin-section observations, the dark-gray mudstone is characterized by higher clay content. Sharp contacts between light- to mid-gray and dark-gray mudstones are commonly observed, associated with intense bioturbation (Figs. 7C, 10H, 10J, 10K, 10N). These contacts are sometimes associated with calcium carbonate cementation. Some packages are characterized by a white spotty texture, attributed to *Chondrites, Phycosiphon* and *Nereites* burrows (Fig. 7B). Remnant laterally discontinuous planar-parallel laminations are observed at microscopic scale, locally characterized by a scoured base (Fig. 8A, B, C, D, E). Grains consist mainly of clay with minor associated quartz, feldspar, organic fragments, and rare zircon and apatite (Fig. 8F). Pyrite nodules are more common than in F1 and F2. In the upper part of the succession near Fan 3, F3 is locally characterized by the presence of outsize coarse mud- to medium sand-sized particles that usually occur as distinct layers in a poorly sorted sandy mud matrix, sometimes associated with remnant bed

contacts (Fig. 9). Outsize particles consist of sub-rounded to sub-angular individual crystals (quartz, altered feldspars, zircons) and composite particles (polycrystalline quartz, foliated metamorphic fragments, mudstone lithics), and range in diameter from 20 µm to 350 µm (long-axis) (Fig. 9). Bioturbation is high to complete (BI: 4-6), and ichnotaxa consist of *Chondrites*, *Helminthopsis*, *Nereites, Phycosiphon*, *Planolites, Teichichnus,* and *Thalassinoides*, which range from 0.1 cm to 6 cm in diameter (Fig. 10). Some burrows are characterized by calcium carbonate cementation (Fig. 10F, K).

Interpretation.--- The discontinuous planar-parallel laminations are interpreted as remnant tractional structures, which suggests original deposition by low-density turbidity currents (*sensu* Lowe 1982) similar to F1 and F2, before reworking by bioturbation. Sections with no laminations may have been deposited by: 1) hemipelagic suspension fallout; or 2) low-density turbidity currents, followed by complete bioturbation. The sharp, intensely bioturbated contacts between light- to mid-gray mudstones and overlying dark-gray mudstones, sometimes associated with early cementation processes, suggest punctuated breaks in sedimentation (Taylor and Curtis 1995; Macquaker and Taylor 1996; Taylor et al. 2000). The origin of outsize coarse mud- to medium sand-sized particles supported by a poorly sorted sandy mud matrix either suggests deposition from: 1) suspension fallout through the water column as dropstones of glacial (ice-rafted debris), or non-glacial origins (e.g. gastroliths, vegetation rafting, aeolian transport) (Bennett et al. 1996); or 2) sediment gravity flows with yield strength, in which coarse mud- to medium sand-sized particles were not vertically segregated from fine mud particles during deposition (i.e. debris flows) (Talling et al. 2012). The clustering, the variable shape and size of the outsize particles, the absence of underlying deformed laminae, and the absence of ice-influenced sedimentation documented in the proximal part of the basin-fill argue against a dropstone interpretation (Bennett et al. 1996). The remnant bed contacts, the poorly sorted matrix, the close stratigraphic association of the outsize particle layers with the sandstone-prone fans, and the common hybrid event beds described in the lobe fringe deposits of the Skoorsteenberg Formation (Hodgson 2009; Kane et al. 2017; Spychala et al. 2017) support the interpretation of the outsize particles as being deposited by low-strength cohesive debris flows (Talling et al. 2012). The pervasive bioturbation, large burrow size, and

relatively high ichnodiversity suggest F3 was deposited under lower sedimentation rate compared to F1 and F2 (Gingras et al. 2011).

FACIES ASSOCIATIONS AND DEPOSITIONAL ENVIRONMENTS

The nine facies described and interpreted in the previous section (including the six in Table 1) combine into five facies associations (FA 1-FA 5), which are linked to five distinct depositional sub-environments on the basin-floor. Illustrations of the five facies associations are shown in Figure 11. Facies and facies association stacking patterns in the OR01 core are shown in Figure 12, and a correlation panel between the different cores is shown in Figure 13. A summary depositional model of the basin-floor fans of the Skoorsteenberg Formation is shown in Figure 14.

Lobe Axis (FA 1), Lobe Off-Axis (FA 2) and Lobe Fringe (FA 3)

The sandstone-prone facies associations are not a primary subject of this study but are summarised here in order to integrate them with the more distal mudstone-prone facies associations. Descriptions and interpretations of lobe axis (FA 1), off-axis (FA 2) and fringe (FA 3) facies associations are based upon current observations integrated with previous sedimentological studies of the Skoorsteenberg Formation (e.g. Morris et al. 2000; Johnson et al. 2001; Hodgson et al. 2006; Luthi et al. 2006; Hodgson 2009; Prélat et al. 2009; Jobe et al. 2012; Hofstra et al. 2015; Spychala et al. 2017; Kane et al. 2017). Lobe axis deposits (FA 1) are 4-8 m thick, and are dominated by structureless sandstones (F4), commonly associated with structured sandstones (F5) and debrites (F7) (Figs. 11A, 12, 14; Table 1). Lobe off-axis deposits (FA 2) are 2-4 m thick, and are dominated by structured sandstones (F5), commonly associated with structureless sandstones (F4) (Figs. 11B, 12, 14). Lobe fringe deposits (FA 3) are 0.1-3 m thick, and consist of very thin- to thin-bedded sandstones (F8), associated with hybrid beds (F6), debrites (F7), structureless sandstones (F4) and structured sandstones (F5) (Figs. 11C, 12, 14). Hybrid beds (F6) are more common in frontal fringe deposits, while very thin- to thin-bedded sandstones (F8) dominate lateral fringe deposits (Spychala et al. 2017). Bioturbation intensity and

ichnodiversity increases from lobe axis to lobe fringe deposits (Fig. 14), which suggest a decrease of physicochemical stressed conditions for organisms from proximal to distal and lateral basin-floor fan environments, potentially linked to lower sedimentation rates and longer depositional breaks (e.g. Heard and Pickering 2008; Gingras et al. 2011).

Lobe Distal Fringe (FA 4)

Description.--- Normally graded mudstones (F1) are commonly associated with faintly bedded mudstones (F2), and rarely with very thin- to thin-bedded sandstones (F8; Table 1) (Figs. 11D, 12). These deposits stack to form 0.05-2.80 m-thick bedsets (*sensu* Campbell 1967), which can be correlated to coeval lobe axis (FA 1), off-axis (FA 2), and fringe (FA 3) deposits (Fig. 13). These bedsets are characterized by a low to high bioturbation index (BI: 1-4), and a relatively low ichnodiversity (*Chondrites*, *Helminthopsis*, *Nereites*, *Phycosiphon* and *Planolites*; Fig. 10). F1 beds are characterized by more common tractional structures (i.e. laminations), lower bioturbation index, and smaller burrows compared to F2 beds.

Interpretation.--- The stacked very thin-bedded nature of F1 and F2, associated with their stratigraphic correlation with lobe axis (FA 1), off-axis (FA 2), and fringe (FA 3) deposits, suggest they represent low-density turbidity current deposits in lobe distal fringe environment (FA 4) (Fig. 14). This interpretation is consistent with the descriptions and interpretations of stacked very thin-bedded mudstones intercalated between lobe axis to fringe deposits from the overlying Fans 3 and 4 of the Skoorsteenberg Formation (Spychala et al. 2017), and from the Unit A deposits of the Laingsburg Formation in the neighbouring Laingsburg depocenter (Prélat and Hodgson 2013). Based on common tractional structures, low bioturbation index, and small burrows, FA 4 deposits are interpreted to be dominated by relatively higher sedimentation rates in the proximal part of the lobe distal fringe environment (Facies F1; Fig. 14), associated with seafloor physicochemically stressed conditions for organisms (e.g. Heard and Pickering 2008; Gingras et al. 2011). Comparatively, FA 4 deposits dominated by higher bioturbation index and larger burrows are consistent with lower depositional rates

in the distal part of the lobe distal fringe environment (Facies F2; Fig. 14), associated with a more favorable seafloor environment for organisms.

Basin-Floor Background (FA 5)

Description.--- Mottled mudstones (F3) form 0.1-10 m thick packages, associated with isolated beds of normally graded mudstone (F1) and faintly bedded mudstone (F2) (Figs. 11E, 12). Metres-thick packages dominated by F3 have been mapped for hundreds of km^2 across the Tanqua depocenter, and do not correlate to any coeval lobe axis (FA 1), off-axis (FA 2) or fringe (FA 3) deposits (Fig. 13). Sections dominated by F3 are characterized by a high to complete bioturbation (BI: 4-6), large burrows, and a relatively high ichnodiversity (*Chondrites*, *Helminthopsis*, *Nereites*, *Phycosiphon*, *Planolites*, *Teichichnus*, *Thalassinoides*; Fig. 10). The metres thick packages are also commonly associated with ash-rich sandstones (F9; Table 1), pyrite nodules and carbonate-rich concretions (Figs. 11E, 12).

Interpretation.--- The mottled texture of the packages dominated by F3, associated with their frequent regional extent, suggests basin-floor background deposits (FA 5) either far from, or in the absence of, coeval lobe sedimentation (Fig. 14). The common remnant tractional structures in FA 5 successions (Fig. 8) suggest that these deposits could have been primarily deposited by low-density turbidity currents. The outsize coarse mud- to medium sand-sized particles in FA 5 (Fig. 9) are closely associated stratigraphically with the sandstone-prone fans (Fig. 12), which suggests deposition by low-strength cohesive debris flows. The high to complete bioturbation, high ichnodiversity and large burrows suggest lower depositional energy and lower frequency of flow events compared to the lobe distal fringe deposits (FA 4), associated with extended periods of favorable and relatively oxygenated seafloor conditions for colonization by organisms (e.g. Heard and Pickering 2008; Gingras et al. 2011; Wetzel and Uchman 2012).

VERTICAL STACKING PATTERNS AND HIERARCHY

Deep-water basin-floor successions are composed of architectural elements, which are defined by their facies associations, bounding surfaces and depositional geometries (e.g. Mutti and Normark 1987; Deptuck et al. 2008; Prélat et al. 2009; MacDonald et al. 2011; Prélat and Hodgson 2013). The different hierarchical orders of genetically-related architectural elements are usually defined using the nature and relative thickness of the enclosing background strata (e.g. Prélat et al. 2009; Flint et al. 2011). Several hierarchical schemes of component architectural elements have been developed for basin-floor fans in order to predict their facies, stacking patterns and spatio-temporal variabilities (e.g. Mutti and Normark 1987; Sprague et al. 2005; Deptuck et al. 2008; Prélat et al. 2009). Prélat et al. (2009) proposed a four-fold outcrop-based hierarchy to stratigraphically subdivide the proximal part of the Skoorsteenberg Formation, using mudstone-prone packages as bounding elements of sandstone-prone architectural elements: 1) a bed represents a single depositional event; 2) one or more beds stack to form a lobe element (<2 m-thick); 3) one or more genetically-related lobe elements separated by very thin- to thin-bedded mudstone-prone packages (<0.02 m-thick) stack to form a lobe (<5 m-thick); 4) one or more genetically-related lobes separated by thicker laterally continuous very thin- to thin-bedded mudstone-prone packages (0.2-2 m-thick) stack to form a lobe complex (up to 50 m-thick). The hierarchy can be extended to the lobe complex set, which consists of one or more genetically-related lobe complexes and represents the lowstand systems tract (e.g. Spychala et al. 2017).

The Prélat et al. (2009) hierarchical scheme has been applied in a variety of proximal basin-floor fan successions, where both sandstones and mudstones are interbedded (e.g. Etienne et al. 2012; Grundvåg et al. 2014; Picot et al. 2016; Terlaky et al. 2016; Pierce et al. 2018). However, the distal basin-floor succession presented in this study is dominated by mudstones (Fig. 13), and thus the mapping of bounding surfaces between sandstone-prone and mudstone-prone packages cannot be used to stratigraphically subdivide the succession. Nonetheless, the distal mudstone-prone basin-floor deposits of the Skoorsteenberg Formation, described above, also display a repetitive vertical organization of facies and facies associations (Figs. 12, 13). Therefore, we developed a new hierarchical approach to stratigraphically subdivide distal mudstone-prone basin-floor deposits, using thickness ranges of basin-

floor background mudstone packages (FA 5) as bounding elements of packages of genetically-related bedded mudstones deposited in lobe distal fringe environments (FA 4) (Fig. 15).

In this study, a bed of F1 and F2 represents the smallest hierarchical order (0.05 to 4 cm thick, with a mean thickness of ~0.2 cm), and is interpreted to represent a single depositional event (Fig. 15). Two or more beds of F1 and F2 stack to form a bedset (*sensu* Campbell 1967) of lobe distal fringe deposits (FA 4) (Figs. 15, 16). Bedsets range in thickness from 0.02-2.80 m, with a mean thickness of 0.15 m. The lower bounding surface of a bedset is a sharp contact of lobe distal fringe deposits (FA 4) over basin-floor background mudstone (FA 5), associated with a decrease of bioturbation intensity, and interpreted as an abrupt increase in sedimentation rate and depositional energy in the basin-floor (Figs. 15, 16). The upper bounding surface of a bedset is a sharp or gradational juxtaposition of basin-floor background mudstones (FA 5), over lobe distal fringe deposits (FA 4), associated with an increase of bioturbation intensity, interpreted as an abrupt decrease in sedimentation rate and depositional energy in the basin-floor (Figs. 15, 16). In 1D (vertical core section), individual bedsets can fine- and thin-upward (Fig. 16A), coarsen- and thicken-upward (Fig. 16B), be disorganized (Fig. 16C), or characterized by an overall constant bed thickness from base to top (Fig. 16D).

In order to identify any hierarchical order of genetically-related bedsets, the range of thicknesses of the enclosing basin-floor background packages (FA 5) have been compiled (Fig. 17). Packages of FA 5 range in thickness from 0.03 to 8.3 m, and a marked decrease in frequency of FA 5 thickness values is identified at 0.7 m (Fig. 17). Thus, we use a FA 5 thickness of 0.7 m as a cut-off value to differentiate two distinct hierarchical orders within this succession: 1) relatively thin packages of basin-floor background deposits (FA 5; <0.7 m thick) separating vertically genetically-related bedsets of lobe distal fringe deposits to form bedset packages; 2) relatively thick packages of basin-floor background deposits (FA 5; >0.7 m thick) separating vertically bedsets or bedset packages that mark different depositional sequences (Figs. 15, 18).

Bedset packages consist of 1 to 16 bedsets, and range in thickness from 0.05-5.50 m, with a mean thickness of 1.3 m (Figs. 15, 18). In 1D (vertical core section), bedset packages exhibit either fining-

and thinning-upward, coarsening- and thickening-upward, coarsening- and thickening-upward followed by fining- and thinning-upward, or are characterized by a disorganized stacking pattern (Fig. 12). The >0.7 m thick background mudstones (FA 5) that separate the bedset packages are more commonly associated with ash-rich sandstones (F9; Table 1), carbonate-rich concretions, pyrite nodules, and outsize grain layers are concentrated near their base or top (Figs. 12, 15, 18). This study is consistent with other studies in the Karoo Basin that used mudstone thickness ranges to define depositional sequence hierarchies in basin-floor deposits (e.g. Flint et al. 2011; Di Celma et al. 2011; Spychala et al. 2017; Brooks et al. 2018); although these studies did not adopt the detailed observational approach used here.

STRATIGRAPHIC ARCHITECTURE

In order to characterize the stratigraphic architecture of the mudstone-prone distal and lateral parts of the Skoorsteenberg Formation, the five cores (OR01, NB2, NB3, NB4 and NS2) have been correlated across the Tanqua depocenter (Fig. 13). The correlation uses the framework from a previous well correlation proposed by Hodgson et al. (2006) that focused mainly on the proximal sandstone-prone part of the system (Fig. 3). NB3 is the most proximal core relative to Fans 1, 2 and 3, while OR01 and NB4 are located in a lateral position, and NB2 and NS2 in a frontal position (Fig. 3) (Johnson et al. 2001; Hodgson et al. 2006). The base of the ~2 m-thick basin-floor background mudstone package (FA 5) underlying Fan 3 has been used as a datum for correlation due to its well-constrained regional extent (Fig. 13) (Hodgson et al. 2006; Prélat et al. 2009). Another correlation marker is the regionally-extensive ~10-15 m-thick basin-floor background package (FA 5) directly overlying Unit 2/3 (Fig. 13) (Hodgson et al. 2006). The bedsets and bedset packages were delineated in each core based on the criteria defined in the previous section: relatively thin FA 5 packages (<0.7 m thick) separate genetically-related bedsets, and thicker FA 5 packages (>0.7 m thick) separate bedset packages. The bedset packages were correlated between the different wells based on the tabularity of basin-floor deposits, and the absence of evidence for significant seafloor topography (Fig. 13).

The correlation below Unit 2/3 is tentative due to the presence of channel-fills in Fans 1 and 2 (Johnson et al. 2001; Hodgson et al. 2006), and post-depositional faults recognized in NB3 (Fig. 13). The lower part of the succession underlying Fan 2 is only penetrated by OR01, and consists of a 108 m-thick section dominated by basin-floor background mudstones (FA 5), with common ash-rich sandstones (F9; Table 1), associated with isolated bedsets of lobe distal fringe deposits (FA 4) (Fig. 12). Some bedsets may correspond to the distal (lateral) fringes of Fan 1 (Fig. 3), and/or to the distal fringes of older lobe complexes. Two bedset packages underlie Fan 2, and together form a laterally persistent thickening-upward succession (Fig. 13). Fan 2 has a maximum thickness of 11.4 m in the proximal position (NB3), where it consists of two sandstone-prone packages, separated by a 0.2 m-thick basin-floor background package (FA 5) (Fig. 13). The lower package of Fan 2 is dominated by lobe axis deposits (FA 1) in proximal position (NB3), that fine and thin to lobe distal fringe deposits (FA 4) in distal (NB2) and lateral (OR01) positions. The upper package of Fan 2 is also dominated by lobe axis deposits (FA 1) in NB3, which fine and thin to off-axis deposits (FA 2) in distal (NB2) and lateral (OR01) positions. Five bedset packages vertically separate Fan 2 and Unit 2/3, and together form an overall thickening- to thinning-upward succession (Fig. 13).

Unit 2/3 has a maximum thickness of 10.4 m in proximal position (NB3), where it consists of a coarsening- and thickening-upward followed by a fining- and thinning-upward sandstone-prone package (Fig. 13). This unit is dominated by lobe axis (FA 1) and off-axis (FA 2) deposits in proximal position (NB3), which fine and thin to lobe distal fringe deposits (FA 4) in distal (NB2) and lateral positions (OR01, NB4) (Fig. 13). The number of bedsets within Unit 2/3 varies laterally from core to core, with five bedsets identified in NB3, seven in OR01, five in NB2, and one in NB4 (Fig. 13). A 10-15 m-thick laterally continuous package of basin-floor background mudstones (FA 5) overlies Unit 2/3, associated with common ash-rich sandstones (F9) (Fig. 13).

The proximity to the datum for correlation and the absence of faults in the section underlying Fan 3 permit a high confidence description of the architecture and facies variability (Fig. 19). The lower four bedset packages together form an overall coarsening- and thickening-upwards then fining- and thinning-upwards succession, while the upper three bedset packages together form a thickening- and coarsening-

upward succession (Fig. 19). The bedset packages are dominated by lobe fringe (FA 3) and distal fringe (FA 4) deposits in proximal position (NB3) (Fig. 19). They fine and thin down dip to NB2 and NS2, and along strike to NB4 and OR01, associated with the sandstone pinchout, and a transition to lobe distal fringe deposits (FA 4) (Fig. 19). This distal and lateral gradation is also associated with a transition from predominantly weakly bioturbated normally graded mudstone (F1) in proximal positions, to predominantly more bioturbated faintly bedded mudstone (F2) in distal and lateral positions (Fig. 19). In the distalmost basin-floor position (NS2), only the uppermost bedset package is identified, while the lower six bedset packages pinchout between NB2 and NS2 (Fig. 19). Within individual bedset packages, the number of bedsets is greatest in the proximal position (NB3), and decreases in distal (NB2, NS2) and lateral (NB4, OR01) positions (Fig. 19). Moreover, the stacking pattern style of individual bedset packages varies laterally from core to core (Fig. 19). For instance, the uppermost bedset package underlying Fan 3 is coarsening- and thickening-upward then fining- and thinning-upward in proximal position (NB3), while it is coarsening- and thickening upward in distal (NB2, NS2) and lateral (NB4, OR01) positions (Fig. 19). The lowermost part of Fan 3 consists of a coarsening- and thickening-upward succession that grade vertically from lobe distal fringe deposits (FA 4), to fringe deposits (FA 3) and to lobe axis (FA 1) or off-axis deposits (FA 2) (Fig. 19).

DISCUSSION

Depositional Processes in Distal Basin-Floor Environments

The distal basin-floor deposits of the Skoorsteenberg Formation, beyond and intercalated with sandstone-prone frontal and lateral lobe fringe deposits, comprise mud deposited in lobe distal fringe (FA 4) and basin-floor background (FA 5) environments (Fig. 14). Differentiation between lobe distal fringe and basin-floor background deposits is easier in core due to exposure limitations and surface weathering in outcrop. The ability to distinguish between mud deposited in lobe distal fringe settings from background mud deposited on the basin-floor beyond a lobe is critical for the paleogeographic

reconstructions of ancient basin-floor successions, and for the correct estimation of lobe dimensions (e.g. Hesse 1975). In our study, lobe distal fringe deposits (FA 4) are dominated by normally graded mudstone (F1) and faintly bedded mudstone (F2), and interpreted to have been deposited by waning, low-density turbidity currents at the distalmost end of lobes. Normally graded mudstones are commonly reported as deposits of distal basin-floor fan successions (e.g. Hesse 1975; Pickering 1981; Etienne et al. 2012; Grundvåg et al. 2014; Baker and Baas 2020; Pickering et al. 2020). These deposits may represent the distal expression of sediment gravity flows that deposited their sand fraction in more proximal slope or basin-floor environments. Alternatively, they may represent the expression of mud-rich low-density turbidity currents originating from the coeval shelf or slope (e.g. Poyatos-Moré et al. 2016; Boulesteix et al. 2019). Some of the very thin beds of F1 are characterized by scoured bases (Fig. 5B), which suggest that low-density turbidity currents in lobe distal fringe locations still have erosive power. These observations indicate that lobe distal fringe environments, commonly associated with low energy deposition and net sediment accumulation by dilute turbidity currents, can still record relatively energetic flows.

The basin-floor background deposits (FA 5), which accumulated either far from, or in the absence of, coeval lobe sedimentation, are dominated by mottled mudstone (F3), with rare isolated normally graded mudstone (F1) and faintly bedded mudstone (F2). In previous studies of the Skoorsteenberg Formation, these mudstones were interpreted as condensed deposits accumulated from hemipelagic settling, based on macroscopic descriptions (Johnson et al. 2001; Hodgson et al. 2006). Similar apparently homogeneous mudstones from other basin-floor successions are also commonly interpreted as hemipelagites (e.g. Hesse 1975; Mutti 1977; Stow and Piper 1984; Baker and Baas 2020). However, basin-floor background deposits are usually highly bioturbated in distal (yet well-oxygenated) basin-floor environments, due to relatively low depositional energy, leading to destruction of the primary sedimentary fabric (e.g. Wetzel and Uchman 2012). Therefore, detailed microscopic descriptions of these otherwise macroscopically homogeneous mudstones are needed to identify potential remnant sedimentary structures indicating primary depositional processes. In our study, the mottled mudstones (F3) are homogeneous at core scale (Fig. 7), and can therefore be easily mistaken as hemipelagites.

However, microscopic observations reveal scours (Fig. 8B, C, E), discontinuous planar-parallel lamination (Fig. 8A, B, D), and outsize coarse mud- to medium sand-sized particles supported by a poorly sorted matrix (Fig. 9). These suggest higher energy primary depositional processes than hemipelagic settling, but commonly overprinted by bioturbation. Laminations in basin-floor mudstones were originally associated with hemipelagic sedimentation and anoxic bottom-water conditions (e.g. Potter et al. 1980; Lundegard and Samuels 1980; Brodie and Kemp 1994). However, flume experiments have shown that bedload transport of coarse mud particles can generate low-angle laminations that have a planar laminated appearance after compaction (Yawar and Schieber 2017). Recent studies of mudstones have started to identify similar sedimentary structures in a wide range of energetic depositional environments (e.g. Schieber and Yawar 2009; Trabucho-Alexandre et al. 2012; Plint 2014; Poyatos-Moré et al. 2016; Schieber 2016). The remnant planar-parallel laminations identified in the basin-floor background mudstone (FA 5) of the Skoorsteenberg Formation suggest that a large proportion of the background mud may have accumulated beyond lobes primarily from low-density turbidity currents, before being reworked by bioturbation. Some packages of FA 5 that immediately underlie and overlie Fan 3 are characterized by layers of outsize particles interpreted as deposited from low-strength cohesive debris flows (Figs. 9, 12). These deposits may result from flow transformation from turbulent to laminar along the flow path (e.g. Kane et al. 2017; Baker and Baas 2020), to concentrate in layers in distal settings. These different observations suggest that background mud along continental margins, commonly interpreted as deposited by continuous and slow hemipelagic settling, may rather accumulate episodically from low-density turbidity currents and rare low-strength cohesive debris flows (e.g. Boulesteix et al. 2019), even in the most down-dip basin-floor positions. The evidence for episodic deposition and reworking of seafloor mud may have major implications for the correct estimation of depositional (and compaction) rates in basin-floor mudstone strata (e.g. Trabucho-Alexandre 2014; Kemp et al. 2018).

Autogenic and Allogenic Controls on Basin-Floor Mud Deposition

The architecture and timing of basin-floor fans is controlled by a complex interplay between allogenic (eustasy, climate, tectonics) and autogenic (channel avulsion, compensational stacking) processes (e.g. Johnson et al. 2001; Hodgson et al. 2006; Prélat et al. 2009; Grundvåg et al. 2014; Blum et al. 2018; Burgess et al. 2019; Sweet et al. 2019; Ferguson et al. 2020). Based on thickness comparison between the architectural elements from the proximal sandstone-prone part of the Skoorsteenberg Formation (bed, lobe element, lobe, lobe complex, lobe complex set; Prélat et al. 2009) and the hierarchical elements from its distal mudstone-prone part described in this study (bed, bedset, bedset package), we tentatively propose that mudstone bedsets may represent the distal expressions of lobe elements and/or lobes, and the mudstone bedset packages may represent the distal expressions of lobe complexes and/or lobe complex sets (Fig. 15). The stratigraphic correlation of mudstone bedsets and bedset packages (FA 4) to coeval sandstone-prone lobe axis (FA 1), off-axis (FA 2) and fringe (FA 3) deposits (Fig. 12), suggests they should also show the influence of both autogenic and allogenic mechanisms, as identified from sandstone-prone deposits elsewhere on the basin-floor (e.g. Prélat et al. 2009). However, some mudstone bedsets and bedset packages may also be the distal expression of disconnected lobes (e.g. Brooks et al. 2018), where mature sediment supply routes were not established, or the distal expression of intraslope lobe complexes (e.g. Spychala et al. 2015), where complex slope topography trapped sand on the slope.

At bedset scale (distal expression of lobe elements and/or lobes), the variable vertical stacking pattern (Fig. 16) could be explained by compensational stacking. Each low-density turbidity current will tend to infill topographic lows on the basin-floor, but also generate subtle topography that will influence the subsequent flows (e.g. Groenenberg et al. 2010). Compensational stacking has been documented in more proximal lobe axis to fringe deposits (e.g. Mutti and Sonnino 1981; Mutti and Normark 1987; Prélat et al. 2009; Groenenberg et al. 2010; Prélat and Hodgson 2013). Therefore, the fining- and thinning-upward bedsets (Fig. 16A) could be explained by successive beds that stack away from a fixed position on the basin-floor, while coarsening- and thickening-upward bedsets (Fig. 16B) can be

explained by successive beds that stack toward a fixed position on the basin-floor (Prélat and Hodgson 2013). A disorganized stacking pattern (Fig. 16C) can be explained by a more variable bed distribution in response to complex seafloor topography. The thin (<0.7 m thick) background mudstone packages (FA 5) that vertically separate genetically-related bedsets of lobe distal fringe deposits (FA 4) suggest a relatively short-term decrease in sedimentation rate and/or sediment supply to certain parts of the basin-floor, while lobe formation was still active elsewhere. Even though an allogenic forcing mechanism (e.g. relative sea-level rise) could result in a similar motif in a vertical 1D section, the limited thickness and extension of the background mudstone packages separating bedsets is more consistent with autogenic up-dip channel avulsion. This would imply that the bounding surfaces of individual bedsets may represent avulsion surfaces.

At a larger scale, the internal stacking pattern of bedset packages (distal expression of lobe complexes and/or lobe complex sets) is highly variable vertically and laterally, with different number of constituent bedsets (lobes and/or lobe elements) from core to core (Fig. 19). Allogenic processes (such as sea-level change or tectonically-induced subsidence) cannot account for the highly variable stacking patterns documented here. This variability may be rather explained by a spatial shift of the bedsets on the basin-floor, forced by autogenic processes such as compensational stacking and/or avulsion of the feeder channel, resulting in a rerouting of sediments to another position on the basin-floor. However, the thicker (>0.7 m thick) and more extensive basin-floor background mudstone packages (FA 5) are commonly associated with ash-rich sandstones (F9; Table 1), the preservation of which suggests long-term and widespread basin-wide decrease in sedimentation rate and sediment supply to the basin-floor. Therefore, where a bedset package is overlain by a >0.7 m thick basin-floor background mudstone package (FA 5), we propose a larger scale, dominantly allogenic control (e.g. relative sea-level rise; see Flint et al. 2011). Following this interpretation, the mudstone bedset package would represent a lowstand systems tract, and the overlying thick basin-floor background mudstone package (FA 5) the combined transgressive and highstand systems tract of a depositional sequence (Johnson et al. 2001; Flint et al. 2011). An accurate dating of the deposits would be useful to test this hypothesis, but the current age model for the Tanqua Karoo deposits is still a matter of debate (see Belica et al. 2017).

Preservation of Event Beds in Deep-Water Mudstones

The proximal sandstone-prone part of Fan 3 of the Skoorsteenberg Formation consists of lobes (axis to fringe), that are 4-10 m thick, and comprise 3 to 10 beds in any one vertical section, with an average bed thickness of 0.5 m (Prélat et al. 2009). Lobe axes are prone to amalgamation and erosion (e.g. Johnson et al. 2001; Hodgson et al. 2006; Prélat et al. 2009), and sediment bypass processes are common in proximal basin-floor environments (e.g. Stevenson et al. 2015). Therefore, the preservation potential of individual event beds is low in lobe axis environments, but progressively increases in lobe off-axis and lobe fringe environments, due to decreasing depositional energy. Even though a sediment gravity flow depositing mud in distal basin-floor environments may have also deposited mud in more proximal environments, mudstones are rarely found in lobe axis to fringe deposits (Figs. 11, 12, 14). This may be explained by the higher energy conditions associated with these proximal lobe sub-environments, as recurrent sediment gravity flows may pick up soft to semi-consolidated mud from the seafloor (rip-up intraclasts) and rework it. This mechanism can explain the very low preservation potential of FA 5 mudstone in proximal basin-floor environments, and the origin of mudstone intraclasts in debrites, as well as the generation of transitional flows and resulting hybrid beds, commonly found in frontal lobe fringe deposits (e.g. Hodgson 2009; Spychala et al. 2017; Kane et al. 2017).

Mudstone bedsets of lobe distal fringe deposits (FA 4) are up to 2.80 m thick with a mean thickness of 0.15 m, and consist of up to several thousand beds, with an average bed thickness of ~0.2 cm (Fig. 15). Therefore, there is a higher number of event beds recorded in mudstone-prone lobe distal fringe deposits compared to their coeval sandstone-prone lobe axis, off-axis, and fringe deposits, due to lower depositional energy. The preservation potential of event beds in distal basin-floor environments is also influenced by the amount of bioturbation disrupting the primary sedimentary fabric, controlled by a range of physicochemical parameters including sedimentation rate, type of substrate, oxygen, food availability and salinity (e.g. Wetzel 1984; Heard and Pickering 2008; Gingras et al. 2011; Wetzel and Uchman 2012). The pervasive bioturbation within the Skoorsteenberg Formation mudstones suggests that oxygen and food availability were not limiting factors for organisms. The proximal part of the lobe

distal fringe deposits (FA 4) is dominated by normally graded mudstone (F1), characterized by sparse to low bioturbation (BI: 1-2), small burrows, and relatively low ichnodiversity (Fig. 14). This suggests that seafloor physicochemical stressed conditions increased with sedimentation rate, without enough time between sedimentary events for organisms to significantly disrupt the newly deposited seafloor mud (e.g. Wetzel 1984; Heard and Pickering 2008; Cummings and Hodgson 2011; Heard et al. 2014). The limited post-depositional bioturbation of the event beds means that most low-density turbidity currents reaching the proximal part of the lobe distal fringe environment are expected to be preserved in the rock record. This suggests that the proximal part of lobe distal fringe deposits (FA 4) are generally good archives to help decipher stratigraphic and paleoenvironmental signals preserved in the deep-water sedimentary record, due to their relatively high stratigraphic completeness compared to more proximal and more distal basin-floor deposits (Fig. 14) (e.g. Weber et al. 2003; Payros et al. 2012; Cantalejo and Pickering 2014; Payros and Martinez-Braceras 2014).

Implications for Dimensions and Geometries of Lobes

Studies of basin-floor fans have commonly focused on their sandstone-prone part (lobe axis, off-axis, fringe), with less understanding of the three-dimensional geometry and extension of deep-water lobes beyond sandstone pinchout. The estimated mean dimension of the sandstone-prone part of lobes from Fan 3 of the Skoorsteenberg Formation is 13 km in width and 27 km in length (Fig. 1) (Prélat et al. 2009). Despite uncertainties about the exact paleogeographic position of the lobe centroids and paleocurrent directions of the bedsets of lobe distal fringe deposits (FA 4) underlying Fan 3 (Fig. 19), a minimum distance to which lobe-scale distal fringe deposits can be traced beyond the sandstone pinchout can be estimated. Paleocurrent indicators from Fan 3 are to the NNE (Hodgson et al. 2006; Prélat et al. 2009; Spychala et al. 2017), and we assume similar paleocurrent directions for the underlying deposits. The bedset underlying Fan 3 is characterized by lobe fringe deposits (FA 3) in proximal positions (NB3), that grade to lobe distal fringe deposits (FA 4) over 18.5 km down dip in a distal position (NS2) (Fig. 19). This distance is taken to be a minimum dip length of lobe distal fringe deposits (FA 4) beyond lobe fringe deposits (FA 3), which suggests that the minimum length of a lobe from the Skoorsteenberg Formation is 45.5 km, including the genetically-linked, mudstone-prone lobe

distal fringe (Fig. 14). Length to width ratio of the sandstone-prone part of Fan 3 is 2.2 (Prélat et al. 2009). By applying a similar ratio for the lobe, including the genetically-linked mudstone-prone distal fringe deposits, the estimated minimum width of a lobe is 20.7 km (Fig. 14). These results suggest that submarine lobes may be much larger than previously estimated, as also suggested by recent flume tank experiments (Spychala et al. 2020). This opens the possibility of identifying (and predicting) the presence or absence of genetically linked deep-water basin-floor sandstone accumulations by the careful examination of deep-water mudstones along basin margin successions.

CONCLUSIONS

A combination of macroscopic and microscopic descriptions of deep-water basin-floor mudstones from the Skoorsteenberg Formation (Karoo Basin, South Africa) indicates that these understudied deposits may be more heterogeneous than previously considered, with implications for basin-floor fan architecture, beyond the sandstone pinchout. Stratigraphic correlation between cored boreholes, supported by previous studies of the continuous regional outcrops, provides a genetic link between the sandstone-prone part of basin-floor fans (lobe axis to fringe), and packages of very thin- to thin-bedded mudstones, interpreted as low-density turbidites accumulated in lobe distal fringe environments. We propose a new hierarchical scheme to stratigraphically subdivide mudstone-prone distal basin-floor successions, using packages of basin-floor background mudstones accumulated either far from, or in the absence of, coeval lobe sedimentation as bounding elements of bedsets and bedset packages of distal fringe deposits. Based on the hierarchical elements previously described in the proximal sandstone-prone part of the Skoorsteenberg Formation, and new hierarchical elements we describe in its distal mudstone-prone part, the bedsets likely represent the distal expressions of lobe elements and/or lobes. The bedset packages likely represent the distal expressions of lobe complexes and/or lobe complex sets. The internal stacking pattern of bedsets and bedset packages of distal fringe deposits is highly variable vertically and laterally, and interpreted as the record of autogenic mechanisms (compensational stacking, avulsion of the feeder channels). Relatively thin background mudstone packages (<0.7 m

thick) separating vertically genetically-related bedsets are interpreted to dominantly represent autogenically-driven lobe abandonment due to up-dip channel avulsion, resulting in local sand starvation in some areas of the basin-floor during lobe complex activity, although with higher preservation potential of short-periods of regional sand starvation. Thicker background mudstone packages (>0.7 m thick) separating vertically bedset packages are interpreted to dominantly represent allogenically-driven changes in sediment supply, resulting in regional sand starvation to the basin-floor, although could include the distal deposits of sand-prone units active for short periods. Remnant tractional structures and outsize particles in the basin-floor background mudstones suggest that low-density turbidity currents and debris flows may agents of mud transport to the basin-floor, challenging the idea that deep-water mud only accumulates through slow and continuous hemipelagic settling in distal settings. The documentation of length scales from lobe fringe to distal fringe deposits suggests that deep-water lobes are much larger than previously estimated, with implications for the paleogeographic reconstructions of ancient basin-floor successions, and for prediction of the presence of genetically-linked deep-water sandstones in up-dip or lateral positions along basin margins. The relatively high preservation potential of event beds in mudstone-prone lobe distal fringe deposits compared to more proximal basin-floor fan settings suggest that these deposits are good archives of stratigraphic and environment signals in deep-water strata.

ACKNOWLEDGEMENTS

REFERENCES

Allen, J.R.L., 1971, Mixing at turbidity current heads, and its geological implications: Journal of Sedimentary Research, v. 41(1), p. 97-113.

Allen, J.R.L., 1973, A classification of climbing-ripple cross-lamination: Journal of the Geological Society, v. 129(5), p. 537-541.

Allen, J.R.L., 1982, Sedimentary Structures: Their Character and Physical Basis, Volumes 1, 2: Amsterdam, Elsevier, 593 p., 663 p.

Arnott, R.W.C., and Hand, B.M., 1989, Bedforms, primary structures and grain fabric in the presence of suspended sediment rain: Journal of Sedimentary Research, v. 59(6), p. 1062-1069.

Baas, J.H., Best, J.L., and Peakall, J., 2011, Depositional processes, bedform development and hybrid bed formation in rapidly decelerated cohesive (mud-sand) sediment flows: Sedimentology, v. 58(7), 1953-1987.

Baker, M.L., and Baas, J.H., 2020, Mixed sand-mud bedforms produced by transient turbulent flows in the fringe of submarine fans: Indicators of flow transformation: Sedimentology.

Belica, M.E., Tohver, E., Poyatos-Moré, M., Flint, S., Parra-Avila, L.A., Lanci, L., Denyszyn, S., and Pisarevsky, S.A., 2017, Refining the chronostratigraphy of the Karoo Basin, South Africa: magnetostratigraphic constraints support an Early Permian age for the Ecca Group: Geophysical Journal International, v. 211(3), p. 1354-1374.

Bennett, M.R. Doyle, P., and Mather, A.E., 1996, Dropstones: their origin and significance: Palaeogeography, Palaoeclimatology, Palaeoecology, v. 121, p. 331-339.

Best, J.L, and Bridge, J., 1992, The morphology and dynamics of low amplitude bedwaves upon upper stage plane beds and the preservation of planar laminae: Sedimentology, v. 39(5), p. 737-752.

Blewett, S., and Phillips, D., 2016, An overview of Cape Fold Belt geochronology: implications for sediment provenance and the timing of orogenesis, *in* Linol, B., and De Wit, M.J., eds., Origin and Evolution of the Cape Mountains and Karoo Basin, Springer, Cham, p. 45-55.

Blum, M., Rogers, K., Gleason, J., Najman, Y., Cruz, J., and Fox, L., 2018, Allogenic and autogenic signals in the stratigraphic record of the deep-sea Bengal Fan: Scientific Reports, v.8(1), p. 1-13.

Bornemann, A., Norris, R.D., Lyman, J.A., D'haenens, S., Groeneveld, J., Röhl, U., Farley, K.A., and Speijer, R.P., 2014, Persistent environmental change after the Paleocene-Eocene Thermal Maximum in the eastern North Atlantic: Earth and Planetary Science Letters, v. 394, p. 70-81.

Boulesteix, K., Poyatos-Moré, M., Flint, S.S., Taylor, K.G., Hodgson, D.M., and Hasiotis, S.T., 2019, Transport and deposition of mud in deep-water environments: Processes and stratigraphic implications: Sedimentology, v. 66(7), p. 2894-2925.

Bouma, A.H., and Wickens H.D.V., 1994, Tanqua Karoo, ancient analog for fine-grained submarine fans. Submarine fans and turbidite systems: GCSSEPM Foundation 15th Annual Research Conference, v. 23, p. 34.

Brodie, I., and Kemp, A.E.S., 1994, Variation in biogenic and detrital fluxes and formation of laminae in late Quaternary sediments from the Peruvian coastal upwelling zone: Marine and Petroleum Geology, v. 116(3-4), p. 385-398.

Bromley, R.G., 1996, Trace Fossils: Biology, Taphonomy and Applications, 2nd edn: Chapman and Hall, London, 361 p.

Brooks, H.L., Hodgson, D.M., Brunt, R.L., Peakall, J., Poyatos-Moré, M., and Flint, S.S., 2018, Disconnected submarine lobes as a record of stepped slope evolution over multiple sea-level cycles: Geosphere, v. 14(4), 1753-1779.

Burgess, P.M., and Hovius, N., 1998, Rates of delta progradation during highstands: consequences for timing of deposition in deep-marine systems: Journal of the Geological Society, v. 155(2), p. 217-222.

Burgess, P.M., Masiero, I., Toby, S.C., and Duller, R.A., 2019, A big fan of signals? Exploring autogenic and allogenic process and product in a numerical stratigraphic forward model of submarine-fan development: Journal of Sedimentary Research, v. 89(1), p. 1-12.

Campbell, C.V., 1967, Lamina, laminaset, bed and bedset: Sedimentology, v. 8(1), p. 7-26.

Cantalejo, B., and Pickering, K.T., 2014, Climate forcing of fine-grained deep-marine systems in an active tectonic setting: Middle Eocene, Ainsa Basin, Spanish Pyrenees: Palaeogeography, Palaeoclimatology, Palaeoecology, v. 410, p. 351-371.

Catuneanu, O., Hancox, P.J., and Rubidge, B.S., 1998, Reciprocal flexural behaviour and contrasting stratigraphies: a new basin development model for the Karoo retroarc foreland system, South Africa: Basin Research, v. 10(4), p. 417-439.

Catuneanu, O., Wopfner, H., Eriksson, P.G., Cairncross, B., Rubidge, B.S., Smith, R.M.H., and Hancox, P.J., 2005, The Karoo basins of south-central Africa: Journal of African Earth Sciences, v. 43(1-3), p. 211-253.

Chukwuma, K., and Bordy, E.M., 2016, Spatiotemporal sedimentary facies variations in the Lower Permian Whitehill Formation, Ecca Group, Karoo Basin, *in* Linol, B., and De Wit, M.J., eds., Origin and Evolution of the Cape Mountains and Karoo Basin, Springer, Cham, p. 101-110.

Cummings, J.P., and Hodgson, D.M., 2011, Assessing controls on the distribution of ichnotaxa in submarine fan environments, the Basque Basin, Northern Spain: Sedimentary Geology, v. 239(3-4), p. 162-187.

De Wit, M.J., and Ransome, I.G.D., 1992, Regional inversion tectonics along the southern margin of Gondwana, *in* De Wit, M.J., and Ransome, I.G.D., eds., Inversion tectonics of the Cape Fold Belt, Karoo and Cretaceous Basins of Southern Africa, p. 15-21.

Deptuck, M.E., Piper, D.J.W., Savoye, B., and Gervais, A., 2008, Dimensions and architecture of late Pleistocene submarine lobes off the northern margin of East Corsica: Sedimentology, v. 55(4), p. 869-898.

Dixon, J.F., Steel, R.J., and Olariu, C., 2012, River-dominated, shelf-edge deltas: delivery of sand across the shelf break in the absence of slope incision: Sedimentology, v. 59(4), p. 1133-1157.

Di Celma, C., Brunt, R.L., Hodgson, D.M., Flint, S.S., and Kavanagh, J.P., 2011, Spatial and temporal evolution of a Permian submarine slope channel-levee system, Karoo Basin, South Africa: Journal of Sedimentary Research, v. 81(8), p. 579-599.

Etienne, S., Mulder, T., Bez, M., Desaubliaux, G., Kwasniewski, A., Parize, O., Dujoncquoy, E., and Salles, T., 2012, Multiple scale characterization of sand-rich distal lobe deposit variability: examples from the Annot Sandstones Formation, Eocene-Oligocene, SE France: Sedimentary Geology, v. 273, p. 1-18.

Ferguson, R.A., Kane, I.A., Eggenhuisen, J.T., Pohl, F., Tilson, M., Spychala, Y.T. and Brunt, R.L., 2020, Entangled external and internal controls on submarine fan evolution: an experimental perspective: Depositional Record.

Flint, S.S., Hodgson, D.M., Sprague, A.R., Brunt, R.L., Van der Merwe, W.C., Figueiredo, J., Prélat, A., Box, D., Di Celma, C., and Kavanagh, J.P., 2011, Depositional architecture and sequence stratigraphy of the Karoo basin floor to shelf edge succession, Laingsburg depocenter, South Africa: Marine and Petroleum Geology, v. 28(3), p. 658-674.

Gingras, M.K., MacEachern, J.A., and Dashtgard, S.E., 2011, Process ichnology and the elucidation of physico-chemical stress: Sedimentary Geology, v. 237(3-4), p. 115-134.

Gomis-Cartesio, L.E., Poyatos-Moré, M., Flint, S.S., Hodgson, D.M., Brunt, R.L., and Wickens, H.D.V., 2016, Anatomy of a mixed-influence shelf edge delta, Karoo Basin, South Africa: Geological Society London, Special Publication, v. 444(1), p. 393-418.

Groenenberg, R.M., Hodgson, D.M., Prelat, A., Luthi, S.M. and Flint, S.S., 2010, Flow–deposit interaction in submarine lobes: Insights from outcrop observations and realizations of a process-based numerical model: Journal of Sedimentary Research, v. 80(3), p. 252-267.

Grundvåg, S.A., Johannessen, E.P, Helland-Hansen, W., and Plink-Björklund, P., 2014, Depositional architecture and evolution of progradationally stacked lobe complexes in the Eocene Central Basin of Spitsbergen: Sedimentology, v. 61(2), p. 535-569.

Hansen, L.A.S., Hodgson, D.M., Pontén, A., Bell, D., and Flint, S.S., 2019, Quantification of basin-floor floor fan pinchouts: examples from the Karoo Basin, South Africa: Frontiers in Earth Science, v. 7.

Haughton, P.D.W., Barker, S.P., and McCaffrey, W.D., 2003, Linked debrites in sand-rich turbidite systems-origin and significance: Sedimentology, v. 50(3), p. 459-482.

Haughton, P.D.W., Davis, C., McCaffrey, W.D., and Barker, S.P., 2009, Hybrid sediment gravity flow deposits – Classification, origin and significance: Marine and Petroleum Geology, v. 26(10), p. 1900-1918.

Heard, T.G., and Pickering, K.T., 2008, Trace fossils as diagnostic indicators of deep-marine environments, Middle Eocene Ainsa-Jaca basin, Spanish Pyrenees: Sedimentology, v. 55(4), p. 809-844.

Heard, T.G., Pickering, K.T., and Clark, J.D., 2014, Ichnofabric characterization of a deep-marine clastic system: a subsurface study of the Middle Eocene Ainsa System, Spanish Pyrenees: Sedimentology, v. 61(5), p. 1298-1331.

Hesse, R., 1975, Turbiditic and non-turbiditic mudstone of Cretaceous flysch sections of the East Alps and other basins: Sedimentology, v. 22(3), p. 387-416.

Hodgson, D.M., Flint, S.S., Hodgetts, D., Drinkwater, N.J., Johannessen, E.P., and Luthi, S.M., 2006, Stratigraphic evolution of a fine-grained submarine fan systems, Tanqua Depocenter, Karoo Basin, South Africa: Journal of Sedimentary Research, v. 76(1), p. 20-40.

Hodgson, D.M., 2009, Distribution and origin of hybrid beds in sand-rich submarine fans of the Tanqua depocentre, Karoo Basin, South Africa: Marine and Petroleum Geology, v. 26(10), p. 1940-1956.

Hofstra, M., Hodgson, D.M., Peakall, J., and Flint, S.S., 2015, Giant scour-fills in ancient channel-lobe transition zones: Formative processes and depositional architecture: Sedimentary Geology, v. 329, p. 98-114.

Huc, A.Y., Bertrand, P., Stow, D.A.V., Gayet, J., and Vandenbroucke, M., 2001, Organic sedimentation in deep offshore settings: the Quaternary sediments approach: Marine and Petroleum Geology, v. 18(4), p. 513-517.

Hunter, R.E., 1977, Terminology of cross-stratified sedimentary layers and climbing-ripple structures: Journal of Sedimentary Research, v. 47(2), p. 697-706.

Jobe, Z.R., Lowe, D.R., and Morris, W.R., 2012, Climbing-ripple successions in turbidite systems: depositional environments, sedimentation rates and accumulation times: Sedimentology, v. 59(3), p. 867–898.

Johnson, M.R., Van Vuuren, C.J., Hegenberger, W.F., Key, R., and Show, U., 1996, Stratigraphy of the Karoo Supergroup in southern Africa: an overview: Journal of African Earth Sciences, v. 23(1), p. 3-15.

Johnson, S.D., Flint, S.S., Hinds, D., and Wickens, H.D.V., 2001, Anatomy, geometry and sequence stratigraphy of basin-floor to slope turbidite systems, Tanqua Karoo, South Africa: Sedimentology, v. 48, p. 987-1023.

Jopling, A.V., and Walker, R.G., 1968, Morphology and origin of ripple-drift cross-lamination, with examples from the Pleistocene of Massachusetts: Journal of Sedimentary petrology, v. 38(4), p. 971-984.

Kane, I.A., and Pontén, A.S.M., 2012, Submarine transitional flow deposits in the Paleogene Gulf of Mexico: Geology, v. 40(12), p. 1119-1122.

Kane, I.A., Pontén, A.S.M., Vangdal, B., Eggenhuisen, J.T., Hodgson, D.M., and Spychala, Y.T., 2017, The stratigraphic record and processes of turbidity current transformation across deep-marine lobes: Sedimentology, v. 64(5), p. 1236-1273.

Kane, I.A., and Clare, M.A., 2019, Dispersion, accumulation, and the ultimate fate of microplatics in deep-marine environments: A review and future directions: Frontiers in Earth Science, v. 7.

Kemp, D.B., Fraser, W.T., and Izumi, K., 2018, Stratigraphic completeness and resolution in an ancient mudrock succession: Sedimentology, v. 65(6), p. 1875-1890.

Kneller, B.C., and Branney, M.J., 1995, Sustained high-density turbidity currents and the deposition of thick massive sands: Sedimentology, v. 42(4), p. 607-616.

Lazar, R.O., Bohacs, K.M., Schieber, J., Macquaker, J.H.S., and Demko, T.M., 2015, Mudstone Primer: Lithofacies variations, diagnostic criteria, and sedimentologic-stratigraphic implications at lamina to bedset scales. SEPM (Society for Sedimentary Geology).

López-Gamundí, O., and Rossello, E.A., 1998, Basin fill evolution and paleotectonic patterns along the Samfrau geosyncline: the Sauce Grande basin-Ventana foldbelt (South Africa) revisited: Geologische Rundschau, v. 86(4), p. 819-834.

Lowe, D.R., 1982, Sediment gravity flows: II, Depositional models with special reference to the deposits of high-density turbidity currents: Journal of Sedimentary Research, v. 52(1), p. 279-297.

Lundegard, P.D., and Samuels, N.D, 1980, Field classification of fine-grained sedimentary rocks: Journal of Sedimentary Research, v. 50(3), p. 781-786.

Luthi, S.M., Hodgson, D.M., Geel, C.R., Flint, S.S., Goedbloed, J.W., Drinkwater, N.J., and Johannessen, E.P., 2006, Contribution of research borehole data to modelling fine grained turbidite reservoir analogues, Permian Tanqua–Karoo basin-floor fans (South Africa): Petroleum Geoscience, v. 12(2), p. 175–190.

MacDonald, H.A., Peakall, J., Wignall, P.B., and Best, J., 2011, Sedimentation in deep-sea lobe-elements: implications for the origin of thickening-upward sequences: Journal of the Geological Society, v. 168(2), p. 319-332.

Macquaker, J.H.S., and Taylor, K.G., 1996, A sequence-stratigraphic interpretation of a mudstone-dominated succession: the Lower Jurassic Cleveland Ironstone Formation, UK: Journal of the Geological Society, London, v. 153(5), p. 759-770.

McCave, I.N., Manighetti, B., and Robinson, S.G., 1995, Sortable silt and fine sediment size/composition slicing: Parameters for palaeocurrent speed and palaeoceanography: Paleoceanography, v. 10(3), p. 593-610.

Middleton, G.V., and Hampton, M.A., 1973, Sediment gravity flows: Mechanics of flow and deposition, *in* Middleton, G.V., Bouma, A.H., eds., Turbidites and deep water sedimentation: Pacific Section. Society of Economic Paleontologists and Mineralogists Book 2, Short Course Notes, p. 1–38.

Migeon, S., Ducassou, E., Le Gonidec, Y., Rouillard, P., Mascle, J., and Revel-Rolland, M., 2010, Lobe construction and sand/mud segregation by turbidity currents and debris flows on the western Nile deep-sea fan (Eastern Mediterranean): Sedimentary Geology, v. 229(3), p. 124-143.

Mignard, S.L.A., Mulder, T., Martinez, P., Charlier, K., Rossignol, L., and Garlan, T., 2017, Deep-sea terrigenous organic carbon transfer and accumulation: Impact of sea-level variations and sedimentation processes off the Ogooue River (Gabon): Marine and Petroleum Geology, v. 85, p. 35-53.

Morris, W.R., Scheilhing, M.H., Wickens, H.D.V., and Bouma, A.H., 2000, Reservoir architecture of deepwater sandstones: examples from the Skoorsteenberg Formation, Tanqua Karoo Sub-Basin, South

Africa, *in* Weimer, P., Slatt, R.M., Bouma, A.H., and Lawrence, D.T., eds., Deep-Water Reservoirs of the World: SEPM, Gulf Coast Section, Twentieth Annual Research Conference, p. 629-666.

Mutti, E., 1977, Distinctive thin-bedded turbidite facies and related depositional environments in the Eocene Hecho Group (South-central Pyrenees, Spain): Sedimentology, v. 24(1), p. 107-131.

Mutti, E., and Sonnino, M., 1981, Compensational cycles: A diagnostic feature of turbidite sandstone lobes (abstract): International Association of Sedimentologists, Second European Regional Meeting, p. 120-123.

Mutti, E., and Normark, W.R., 1987, Comparing examples of modern and ancient turbidite systems: problems and concepts, *in* Leggett, J.K., and Zuffa, G.G., eds., Marine Clastic Sedimentology: Concepts and Case Studies: Boston, Graham and Trotman, p. 1-38.

Normark, W.R., 1970, Growth patterns of deep-sea fans: AAPG Bulletin, v. 54, p. 2170-2195.

Payros, A., Ortiz, S., Alegret, L., Orue-Etxebarria, X., Apellaniz, E., and Molina, E., 2012, An early Lutetian carbon-cycle perturbation: Insights from the Gorrondatxe section (western Pyrenees, Bay of Biscay): Paleoceanography and Paleoclimatology, v. 27(2).

Payros, A., and Martínez-Braceras, N., 2014, Orbital forcing in turbidite accumulation during the Eocene greenhouse interval: Sedimentology, v. 61(5), p. 1411-1432.

Pickering K.T., 1981, Two types of outer fan lobe sequence, from the late Precambrian Kongsfjord Formation submarine fan, Finnmark, North Norway: Journal of Sedimentary Research, v. 51(4), p. 1277-1286.

Pickering, K.T., Pouderoux, H., McNeill, L.C., Backman, J., Chemale, F., Kutterolf, S., Milliken, K.L., Mukoyoshi, H., Henstock, T.J., Stevens, D.E., Parnell, C., and Dugan, B., 2020, Sedimentology, stratigraphy and architecture of the Nicobar Fan (Bengal-Nicobar Fan System), Indian Ocean: Results from International Ocean Discovery Program Expedition 362: Sedimentology, v. 67(5), p. 2248-2281.

Picot, M., Droz, L., Marsset, T., Dennielou, B., and Bez, M., 2016, Controls on turbidite sedimentation: insights from a quantitative approach of submarine channel and lobe architecture (Late Quaternary Congo Fan): Marine and Petroleum Geology, v. 72, p. 423-446.

Pierce, C.S., Haughton, P.D.W., Shannon, P.M., Pulham, A.J., Barker, S.P., and Martinsen, O.J., 2018, Variable character and diverse origin of hybrid event beds in a sandy submarine fan system, Pennsylvanian Ross Sandstone Formation, western Ireland: Sedimentology, v. 65(3), p. 952-992.

Piper, D.J.W., 1978, Turbidite muds and silts on deep-sea fans and abyssal plains, *in* Stanley, D.J., and Kelling, G., eds., Sedimentation in Submarine Canyons, Fans, and Trenches: Stroudsburg, Pennsylvania, Dowden, Hutchinson & Ross, p. 163-176.

Plint, G.A., 2014, Mud dispersal across a Cretaceous prodelta: Storm-generated, wave-enhanced sediment gravity flows inferred from mudstone microtexture and microfacies: Sedimentology, v. 61(3), p. 609-647.

Pohl, F., Eggenhuisen, J.T., Kane, I.A., and Clare, M.A., 2020, Transport and burial of microplastics in deep-marine sediments by turbidity currents: Environmental Science & Technology, v. 54(7), p. 4180-4189.

Potter, P.E., Maynard, J.B., and Pryor, W.A., 1980, Sedimentology of Shale: New York, Springer-Verlag, 306 p.

Poyatos-Moré, M., Jones, G.D., Brunt, R.L., Hodgson, D.M., Wild, R.J., and Flint, S.S., 2016, Mud-dominated basin-margin progradation: Processes and implications: Journal of Sedimentary Research, v. 86(8), p. 863-878.

Prélat, A., Hodgson, D.M., and Flint, S.S., 2009, Evolution, architecture and hierarchy of distributary deep-water deposits: a high resolution outcrop investigation from the Permian Karoo Basin, South Africa: Sedimentology, v. 56(7), p. 2132-2154.

Prélat, A., and Hodgson, D.M., 2013, The full range of turbidite bed thickness patterns in submarine lobes: controls and implications: Journal of the Geological Society, London, v. 170(1), p. 209-214.

Pysklywec, R.N., and Mitrovica, J.X., 1999, The role of subduction-induced subsidence in the evolution of the Karoo Basin: The Journal of Geology, v. 107(2), p. 155-164.

Satur, N., Hurst, A., Cronin, B.T., Kelling, G., and Gürbüz, K., 2000, Sand body geometry in a sand-rich, deep-water clastic system, Miocene Cingöz Formation of southern Turkey: Marine and Petroleum Geology, v. 17(2), p. 239-252.

Schieber, J., and Yawar, Z., 2009, A new twist on mud deposition – Mud ripples in Experiment and rock record: The Sedimentary Record, v. 7(2), p. 4-8.

Schieber, J., 2016, Mud-redistribution in epicontinental basins – Exploring likely processes: Marine and Petroleum Geology, v. 71, p. 119-133.

Schmitz, B., Pujalte, V., and Núñez-Betelu, K., 2001, Climate and sea-level perturbations during the incipient Eocene Thermal Maximum: evidence from siliciclastic units in the Basque Basin (Ermua, Zumaia and Trabakua Pass), northern Spain: Palaeogeography, Palaeoclimatology, palaeoecology, v. 165(3-4), p. 299-320.

Smith, R.M.H., 1990, A review of stratigraphy and sedimentary environments of the Karoo Basin of South Africa: Journal of African earth Sciences, v. 16(1-2), p. 117-137.

Southard, J.B., 1991, Experimental determination of bed-form stability: Annual Review of Earth and Planetary Sciences, v. 19(1), p. 423-455.

Sprague, A.R.G., Garfield, T.R., Goulding, F.J., Beaubouef, R.T., Sullivan, M.D., Rossen, C., Campion, K.M., Sickafoose, D.K., Abreu, V., Schellpeper, M.E., Jensen, G.N., Jennette, D.C., Pirmez, C., Dixon, B.T., Ying, D., Ardill, J., Mohrig, D.C., Porter, M.L., Farrell, M.E., and Mellere, D., 2005, Integrated slope channel depositional models: The key to successful prediction of reservoir presence and quality

in offshore West Africa: CIPM, Cuarto E-Exitep 2005, February 20–23, 2005, Veracruz, Mexico, pp. 1–13.

Spychala, Y.T., Hodgson, D.M., Flint, S.S., and Mountney, N.P., 2015, Constraining the sedimentology and stratigraphy of submarine intraslope lobe deposits using exhumed examples from the Karoo Basin, South Africa: Sedimentary Geology, v. 322, p. 67-81.

Spychala, Y.T., Hodgson, D.M., Prélat, A., Kane, I.A., Flint, S.S., and Mountney, N.P., 2017, Frontal and lateral submarine lobe fringes: Comparing sedimentary facies, architecture and flow processes: Journal of Sedimentary Research, v. 87(1), p. 75-96.

Spychala, Y.T., Eggenhuisen, J.T., Tilston, M., and Pohl, F., 2020, The influence of basin setting and turbidity current properties on the dimensions of submarine lobe elements. Sedimentology.

Stevenson, C.J., Jackson, C.A.L., Hodgson, D.M., Hubbard, S.M., and Eggenhuisen, J.T., 2015, Deep-water sediment bypass: Journal of Sedimentary Research, v. 85(9), p. 1058-1081.

Stow, D.A.V., and Shanmugam, G., 1980, Sequence of structures in fine-grained turbidites: comparison of recent deep-sea and ancient flysch sediments: Sedimentary Geology, v. 25(1-2), p. 23-42.

Stow, D.A.V., and Piper, D.J.W, 1984, Deep-water fine-grained sediments: facies models: Geological Society, London, Special Publications, v. 15(1), p. 611-646.

Sweet, M.L., Gaillot, G.T., Jouet, G., Rittenour, T.M., Toucanne, S., Marsset, T., and Blum, M.D., 2019, Sediment routing from shelf to basin floor in the Quaternary Golo System of Eastern Corsica, France, western Mediterranean Sea: GSA Bulletin.

Talling, P.J., Masson, D.G., Sumner, E.J., and Malgesini, G., 2012, Subaqueous sediment density flows: Depositional processes and deposit types: Sedimentology, v. 59(7), p. 1937-2003.

Talling, P.J., 2013, Hybrid submarine flows comprising turbidity current and cohesive debris flows: deposits, theoretical and experimental analyses, and generalized models: Geosphere, v. 9(3), p. 460-488.

Tankard, A., Welsink, H., Aukes, P., Newton, R., and Stettler, E., 2009, Tectonic evolution of the Cape and Karoo basins of South Africa: Marine and Petroleum Geology, v. 26(8), p. 1379-1412.

Tankard, A., Welsink, H., Aukes, P., Newton, R., and Stettler, E., 2012, Geodynamic interpretation of the Cape and Karoo basins, South Africa, *in* Regional Geology and Tectonics: Phanerozoic Passive Margins, Cratonic Basins and Global Tectonic Maps, Elsevier, p. 868-945.

Taylor, A.M. and Goldring, R., 1993, Description and analysis of bioturbation and ichnofabric: Journal of the Geological Society, v. 150(1), p. 141-148.

Taylor, K.G., and Curtis, C.D., 1995, Stability and facies association of early diagenetic mineral assemblages: an example from a Jurassic ironstone-mudstone succession, UK: Journal of Sedimentary Research, v. 65(2), p. 358-368.

Taylor, K.G., Gawthorpe, R.L., Curtis, C.D., Marshall, J.D., and Awwiller, D.N., 2000, Carbonate cementation in a sequence-stratigraphic framework: Upper Cretaceous Sandstones, Book Cliffs, Utah-Colorado: Journal of Sedimentary Research, v. 70(2), p. 360-372.

Terlaky, V., Rocheleau, J., and Arnott, R.W.C., 2016, Stratal composition and stratigraphic organization of stratal elements in an ancient deep-marine basin-floor succession, Neoproterozoic Windermere Supergroup, British Columbia, Canada: Sedimentology, v. 63(1), p. 136-175.

Trabucho-Alexandre, J., Dirkx, R., Veld, H., Klaver, G., and De Boer, P.L., 2012, Toarcian black shales in the Dutch Central Graben: record of energetic, variable depositional conditions during an oceanic anoxic event: Journal of Sedimentary Research, v. 82(2), p. 104-120.

Trabucho-Alexandre, J. 2014, More gaps than shale: erosion of mud and its effect on preserved geochemical and palaeobiological signals. In: Smith, D. G., Bailey, R. J., Burgess, P. M. and Fraser, A.J. (eds) Strata and Time: Probing the Gaps in Our Understanding. Geological Society, London, Special Publications, v. 404, p. 251-270.

Veevers, J.J., Cole, D.I., and Cowan, E.J., 1994, Southern Africa: Karoo Basin and Cape Fold Belt, *in* Veevers, J.J., and Powell, C.M., eds., Permian-Triassic Pangean Basins and foldbelts along the Panthalassan margin of Gondwanaland, The Geological Society of America, Boulder, CO. Geological Society America, Memoir, v. 184, p. 223-279.

Viglietti, P.A., Rubidge, B.S., and Smith, R.M., 2017, New Late Permian tectonic model for South Africa's Karoo Basin: foreland tectonics and climate change before the end-Permian crisis: Scientific Reports, v. 7(1), p. 1-7.

Viljoen, J.H.A., 1994, Sedimentology of the Collingham Formation, Karoo Supergroup: South African Journal of Geology, v. 97(2), p. 167-183.

Visser, J.N.J., 1992, Deposition of the early to late Permian Whitehill Formation during a sea-level highstand in a juvenile foreland basin: South African Journal of Geology, v. 95 (5-6), p. 181-193.

Visser, J.N.J., and Praekelt, H.E., 1996, Subduction, mega-shear systems and Late Palaeozoic basin development in the African segment of Gondwana: Geologische Rundschau, v. 85(4), p. 632-646.

Weber, M.E., Wiedicke-Hombach, M., Kudrass, H.R., and Erlenkeuser, H., 2003, Bengal Fan sediment transport activity and response to climate forcing inferred from sediment physical properties: Sedimentary Geology, v. 155(3-4), p. 361-381.

Wetzel, A., 1984, Bioturbation in deep-sea fine-grained sediments: influence of sediment texture, turbidite frequency and rates of environmental change: Geological Society, London, Special Publications, v. 15(1), p. 595-608.

Wetzel, A., and Uchman, A., 2012, Hemipelagic and pelagic basin plains, *in* Developments in Sedimentology, v. 64, p. 673-701. Elsevier.

Wickens, H.D.V., 1994, Basin-floor fan building turbidites of the southwestern Karoo Basin, Permian Ecca Group, South Africa [PhD Thesis]: University of Port Elizabeth, Port Elizabeth, South Africa, 233 p.

Wild, R., Flint, S.S., and Hodgson, D.M., 2009, Stratigraphic evolution of the upper slope and the shelf edge in the Karoo Basin, South Africa: Basin Research, v. 21(5), p. 502-527.

Yawar, Z., and Schieber, J., 2017, On the origin of silt laminae in laminated shale: Sedimentary Geology, v. 360, p. 22-34.
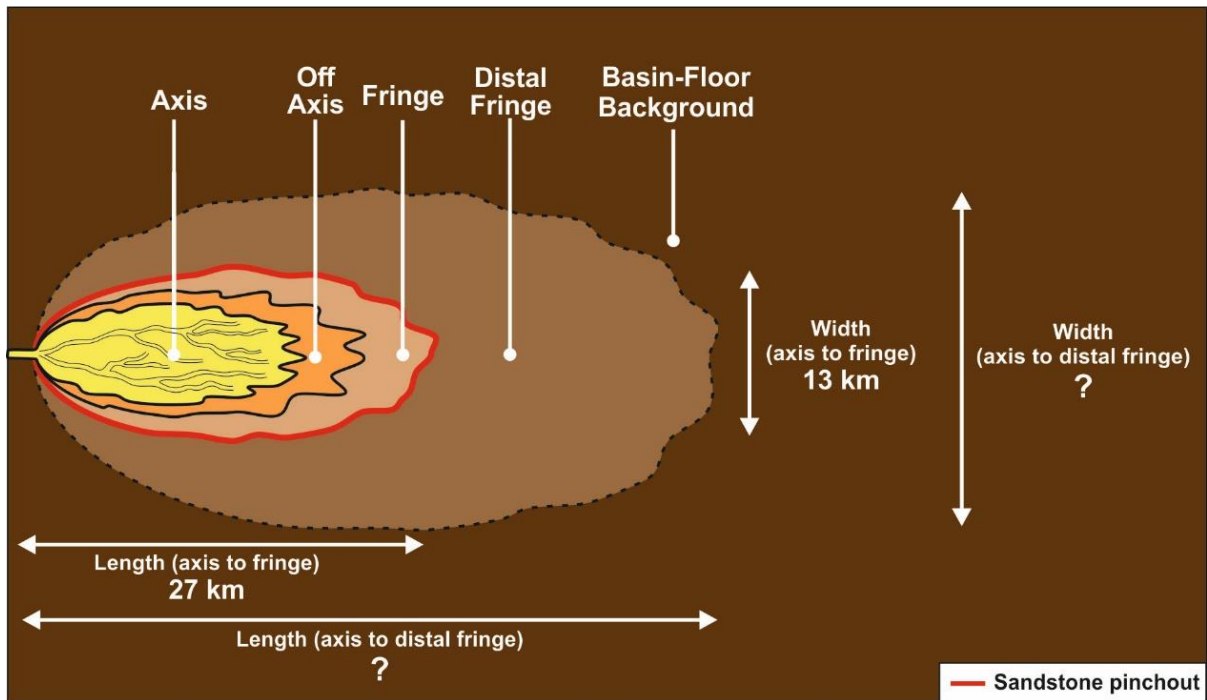
Figure 1: Simplified planform view of lobe sub-environments (axis, off-axis, fringe, distal fringe). Average lobe dimensions are from Fan 3 of the Skoorsteenberg Formation (Karoo Basin, Tanqua depocenter). Redrawn from Prélat et al. (2009).
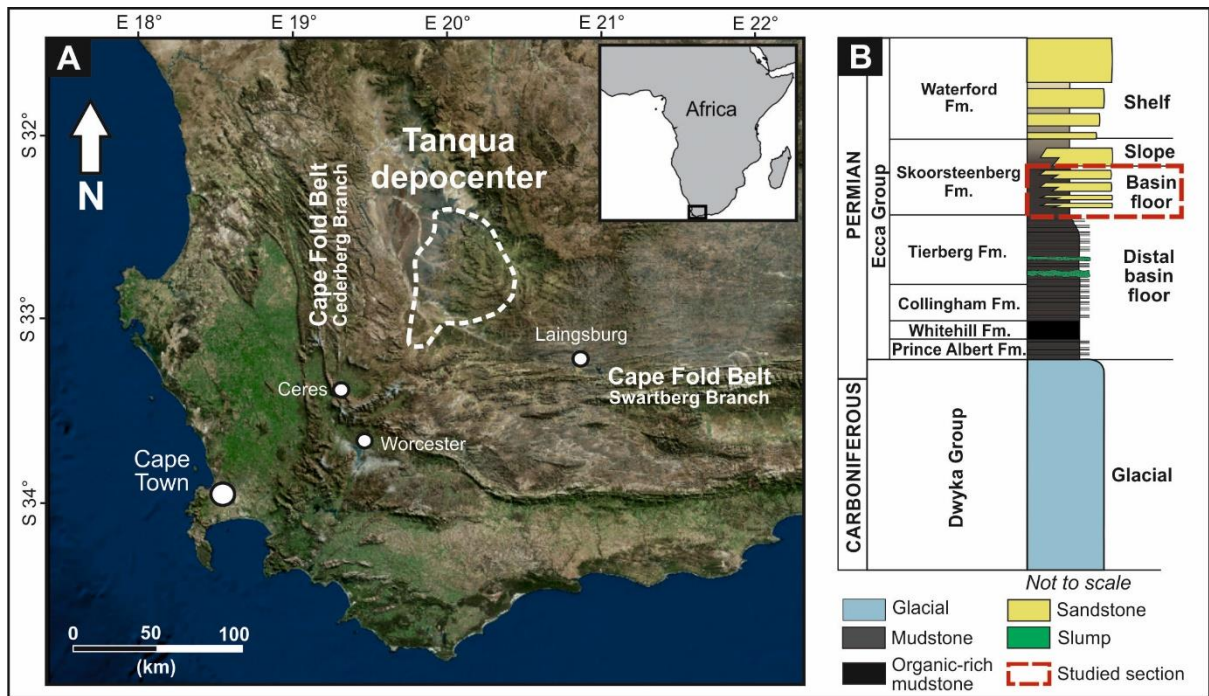
Figure 2: A) Satellite view of southwest South Africa with location of the study area (Tanqua depocenter, Karoo Basin) indicated by the white dotted line. **B)** Schematic stratigraphic log of the Karoo Supergroup in the Tanqua depocenter. The stratigraphy presented in this study is indicated by the red dotted square. Modified after Wickens (1994).
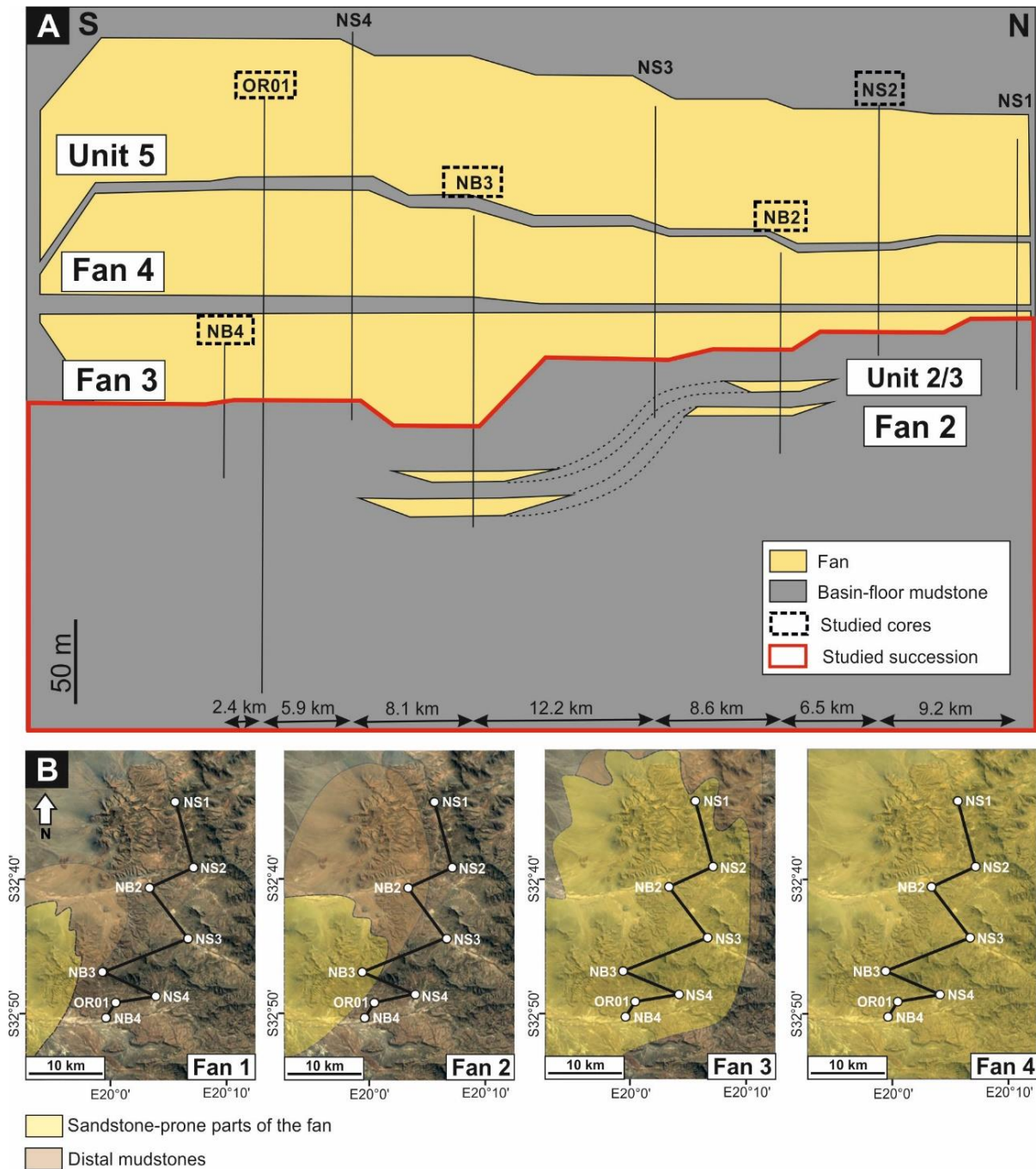
Figure 3: A) Simplified correlation panel of Fans 2-4 and Unit 5. Fan 1 is not encountered in the subsurface dataset. The apparent lens shape of Fan 2 and Unit 2/3 is due to the change of direction of correlation. The red square indicates the succession presented in this study. Modified after Hodgson et al. (2006). **B)** Satellite view of the study area (Tanqua depocenter) with interpreted paleogeographical extent of Fans 1-4. Interpretation based on outcrops mapping integrated with core analysis. Modified after Hodgson et al. (2006) and Hansen et al. (2019).

	Core	**Thin Section**
Facies 1 Normally graded mudstone	A · Fig. 4B · 1 cm	B · 5 mm · Planar-parallel laminations · Flame structure · Planar-parallel laminations
Facies 2 Faintly bedded mudstone	C · Fig. 4D · 1 cm	D · 5 mm · Gradational bed contact · Normal grading
Facies 3 Mottled mudstone	E · Fig. 4F · 1 cm	F · 5 mm · Remnant laminations · Pyrite nodules

47
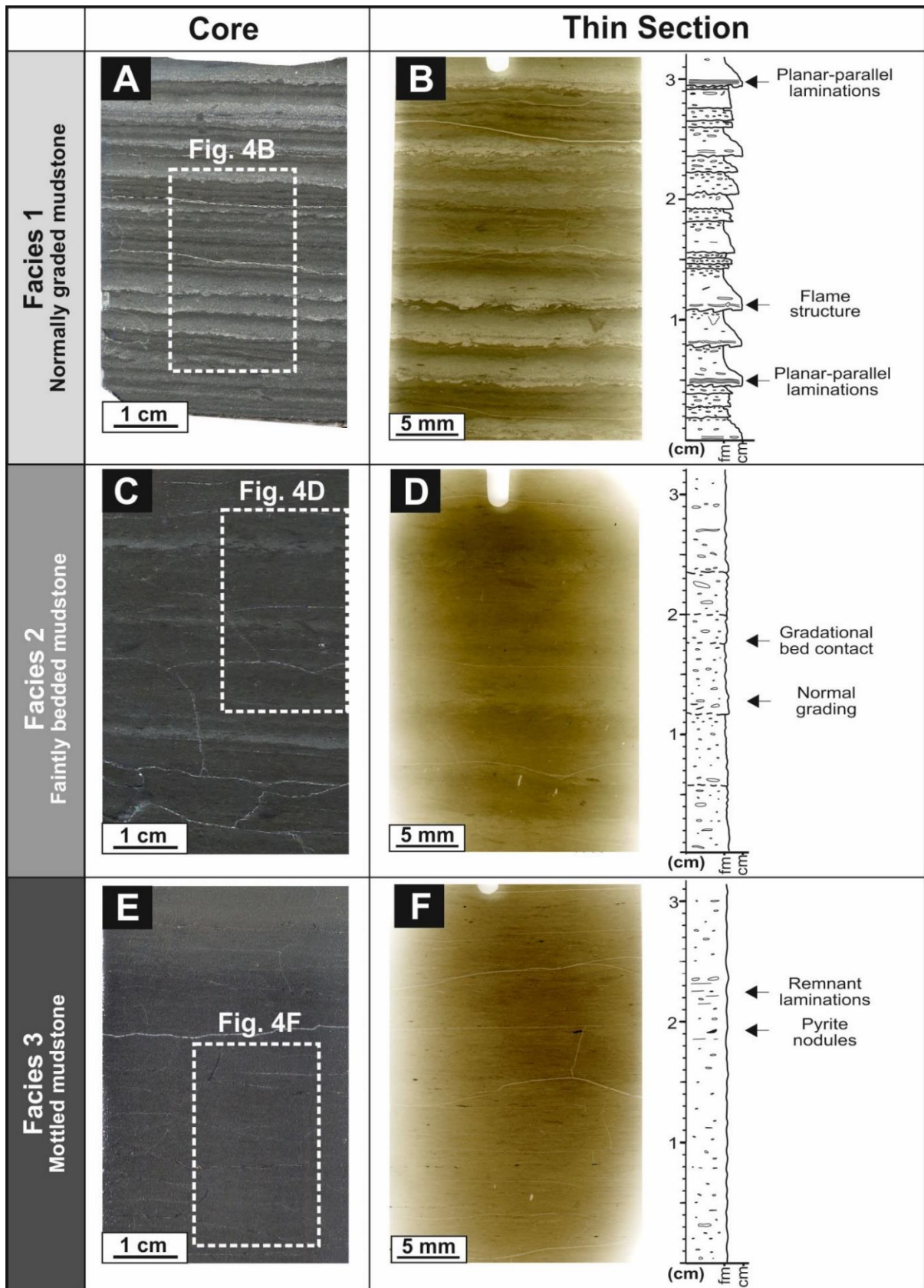
Figure 4: Illustrations of the three mudstone facies identified in the Skoorsteenberg Formation (from OR01 core). A, C and E are dry core photographs. B, D and F are thin-section scans with microstratigraphic logs. White dotted squares in core views indicate locations of thin sections. **A)** Facies 1 (normally graded mudstone) characterized by stacked very thin beds (260.11 m). **B)** Stacked normally graded very thin mudstone beds with sharp or erosional base. Planar-parallel laminations are only observed at the base of the thickest beds. Bioturbation is sparse to low (BI: 1-2). Note the flame structures at the base of the beds. **C)** Facies 2 (faintly bedded mudstone) characterized by laterally discontinuous beds (291.74 m). **D)** Upper and lower bed contacts are gradational due to strong bioturbation. Rare preserved normal grading. Bioturbation is high (BI: 4). **E)** Facies 3 (mottled mudstone) with homogeneous texture at core scale (148.71 m). **F)** Mottled texture with common pyrite nodules and remnant laminations.
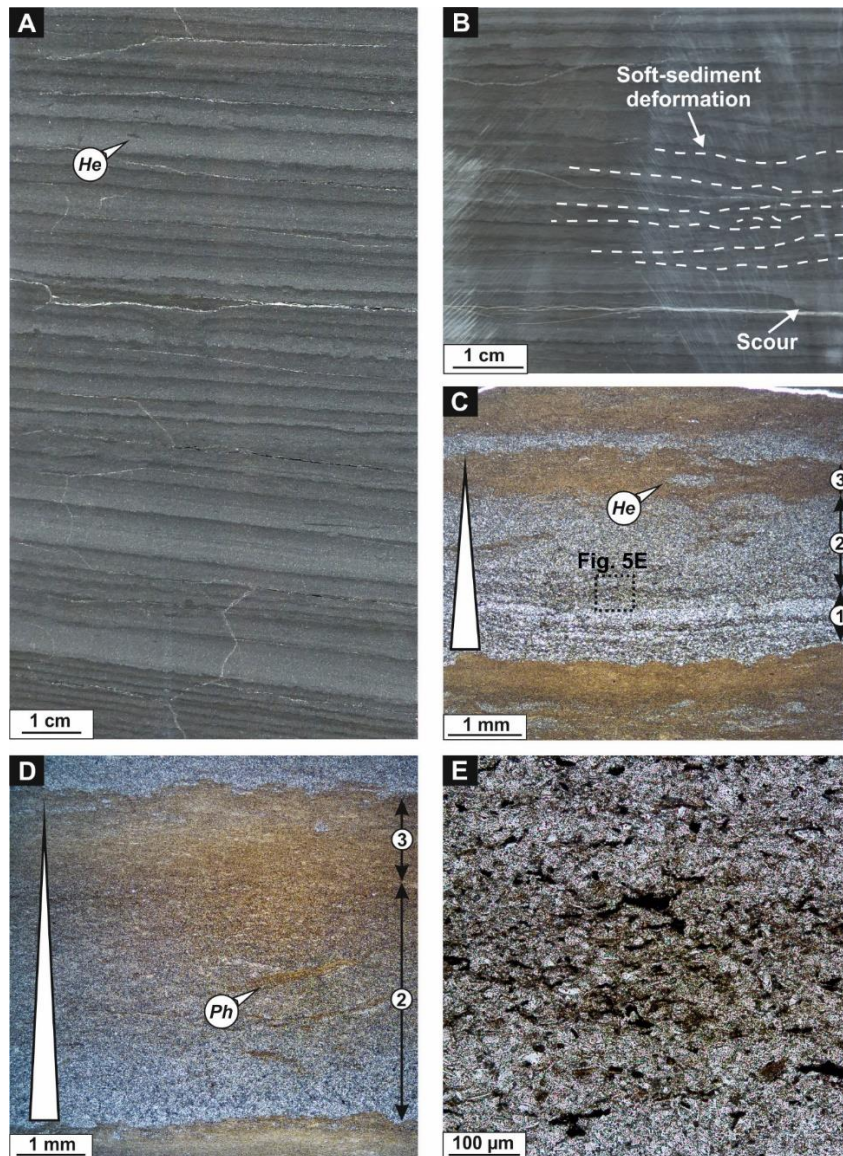
Figure 5: Facies 1 (normally graded mudstone) examples of key features (from OR01 core). A and B are wet core photographs. C, D and E are photomicrographs (plane-polarized light). *He = Helminthopsis*; *Ph = Phycosiphon*. **A)** Stacked normally graded very thin beds (265.55 m). Note the upward decrease of bed dip angle and the sparse to low bioturbation (BI: 1-2). **B)** Stacked normally graded very thin beds associated with a scour and soft-sediment deformation (285.70 m). **C)** Tripartite erosional normally graded very thin bed (145.03 m). The lower subdivision (1) consists of laterally continuous to discontinuous planar-parallel laminated coarse mudstone. The middle subdivision (2) consists of normally graded coarse mudstone. The upper subdivision (3) consists of ungraded mottled fine mudstone. **D)** Bipartite erosional normally graded very thin bed (215.08 m). The lower subdivision (2) consists of normally graded fine mudstone while the upper subdivision (3) consists of ungraded mottled fine mudstone. **E)** Magnified view of the lower subdivision of the bed presented in Figure 5C (145.03 m). Grains consist of quartz, feldspar, clay, and organic fragment, with minor zircon and apatite.
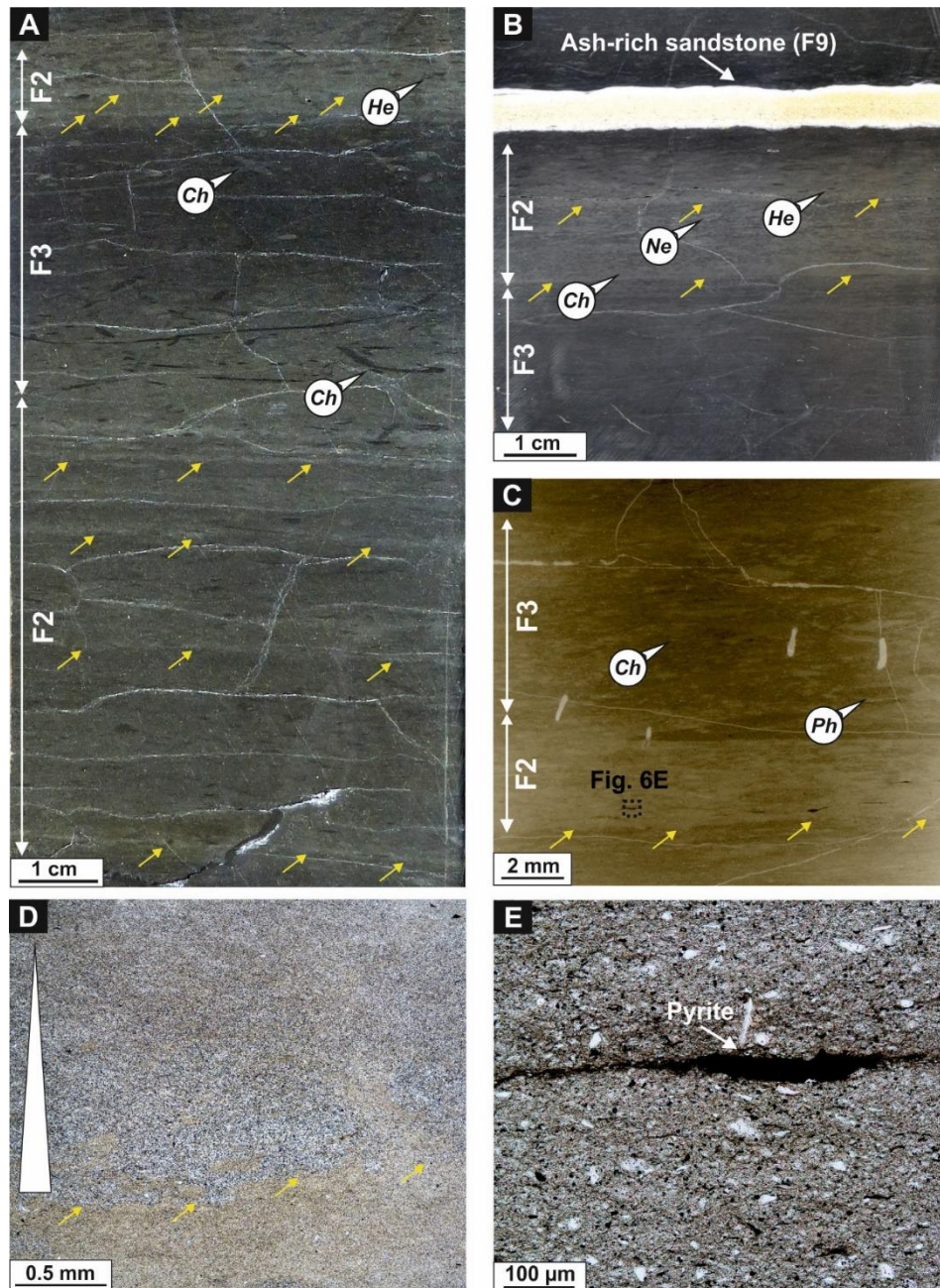
Figure 6: Facies 2 (faintly bedded mudstone) examples of key features (from OR01 core). A and B are wet core photographs. C is a thin-section scan. D and E are photomicrographs (plane-polarized light). Yellow arrows indicate the base of mudstone beds. *Ch = Chondrites*; *He = Helminthopsis*; *Ne = Nereites; Ph = Phycosiphon*. **A)** Stacked faint very thin mudstone beds (218.13 m). Note darker package of Facies 3 with homogeneous texture. **B)** Two stacked faint very thin mudstone beds (363.44 m). **C)** Detail of a faint very thin bed (374.25 m). The lower contact is bioturbated, and the bed is ungraded because of intense bioturbation. The bed grades to Facies 3. **D)** Normally graded very thin mudstone bed with a gradational bioturbated lower contact (291.74 m). **E)** Magnified view of the lower subdivision of the bed presented in Figure 6C (374.25 m). Grains consist of clay, quartz, feldspar and organic fragment. Note the pyrite at the middle of the photomicrograph.
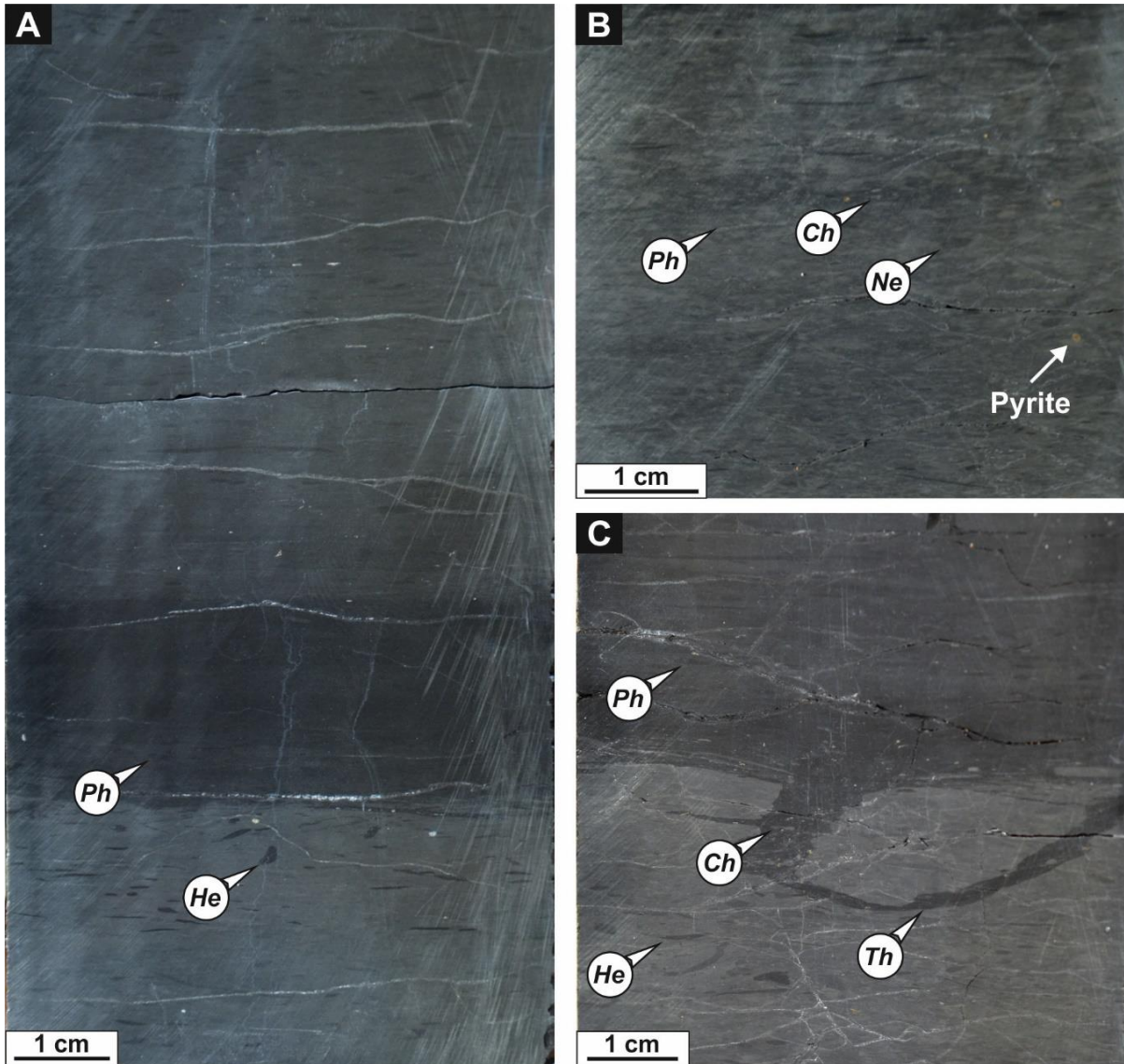
Figure 7: Facies 3 (mottled mudstone) examples of macroscopic key features (from OR01 core). A, B and C are wet core photographs. *Ch = Chondrites*; *He = Helminthopsis*; *Ne = Nereites; Ph = Phycosiphon; Th = Thalassinoides*. **A)** Mottled mudstone with intercalated dark- and mid-gray packages with gradational contacts (237.90 m). **B)** Mottled mudstone with white spotty texture attributed to *Phycosiphon*, *Chondrites* and *Nereites* burrows (298.10 m). **C)** Sharp transition from mid- to dark-gray mudstone, associated with intense bioturbation (345.30 m).
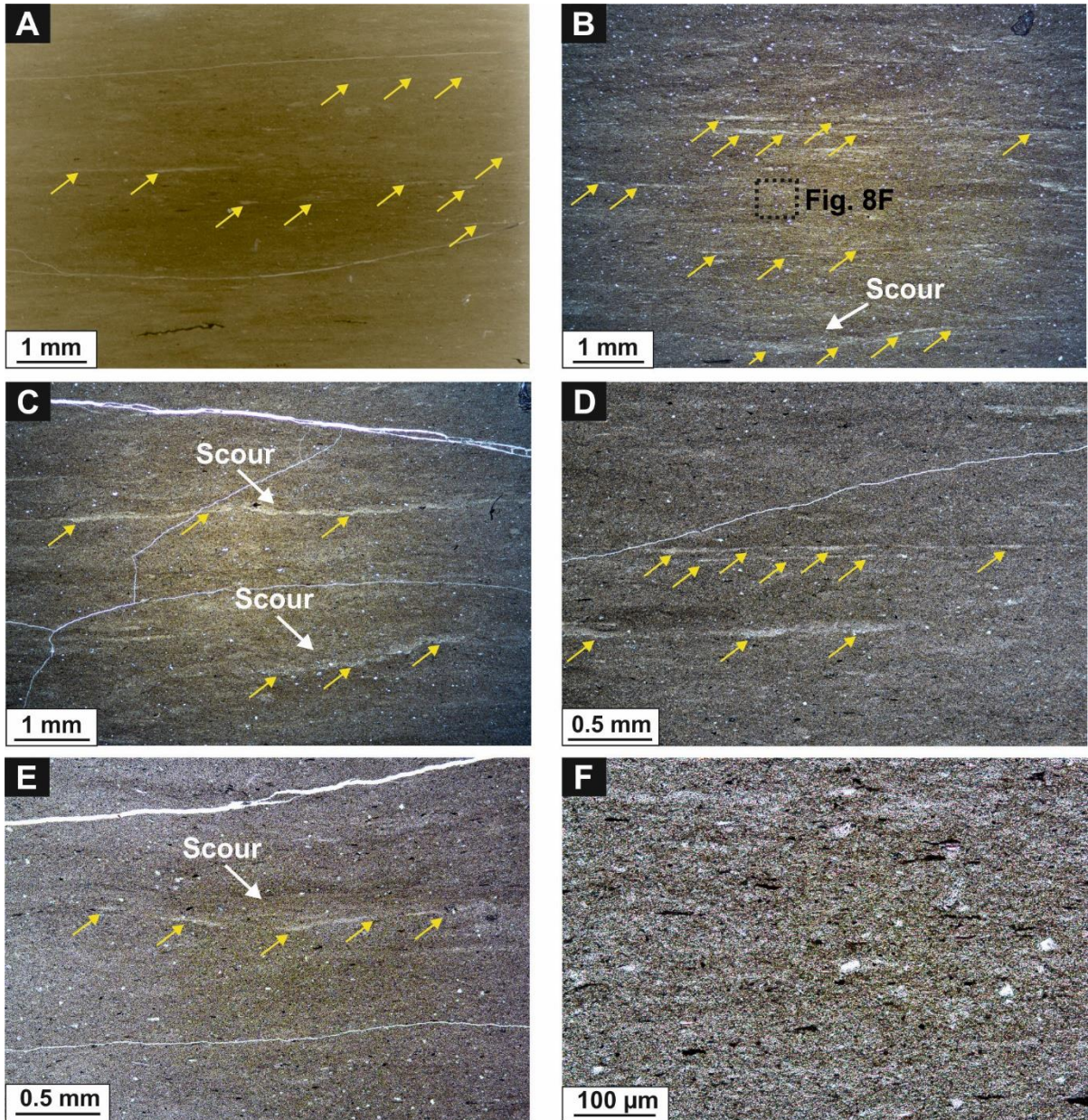
Figure 8: Facies 3 (mottled mudstone) examples of microscopic key features (from OR01 core). A is a thin-section scan. B, C, D, E and F are photomicrographs (plane-polarized light). Discontinuous laminations and scours are indicated by yellow arrows. **A)** Discontinuous laminations (237.55 m). **B)** Discontinuous laminations (147.80 m). The basal lamination is characterized by a scoured base. **C)** Discontinuous laminations with scoured base (261.63 m). **D)** Discontinuous laminations (244.41 m). **E)** Discontinuous lamination with a scoured base (348.20 m). **F)** Zoom on the microscopic view presented in Figure 8B. Grains consist of clay, quartz, feldspar and organic fragment.
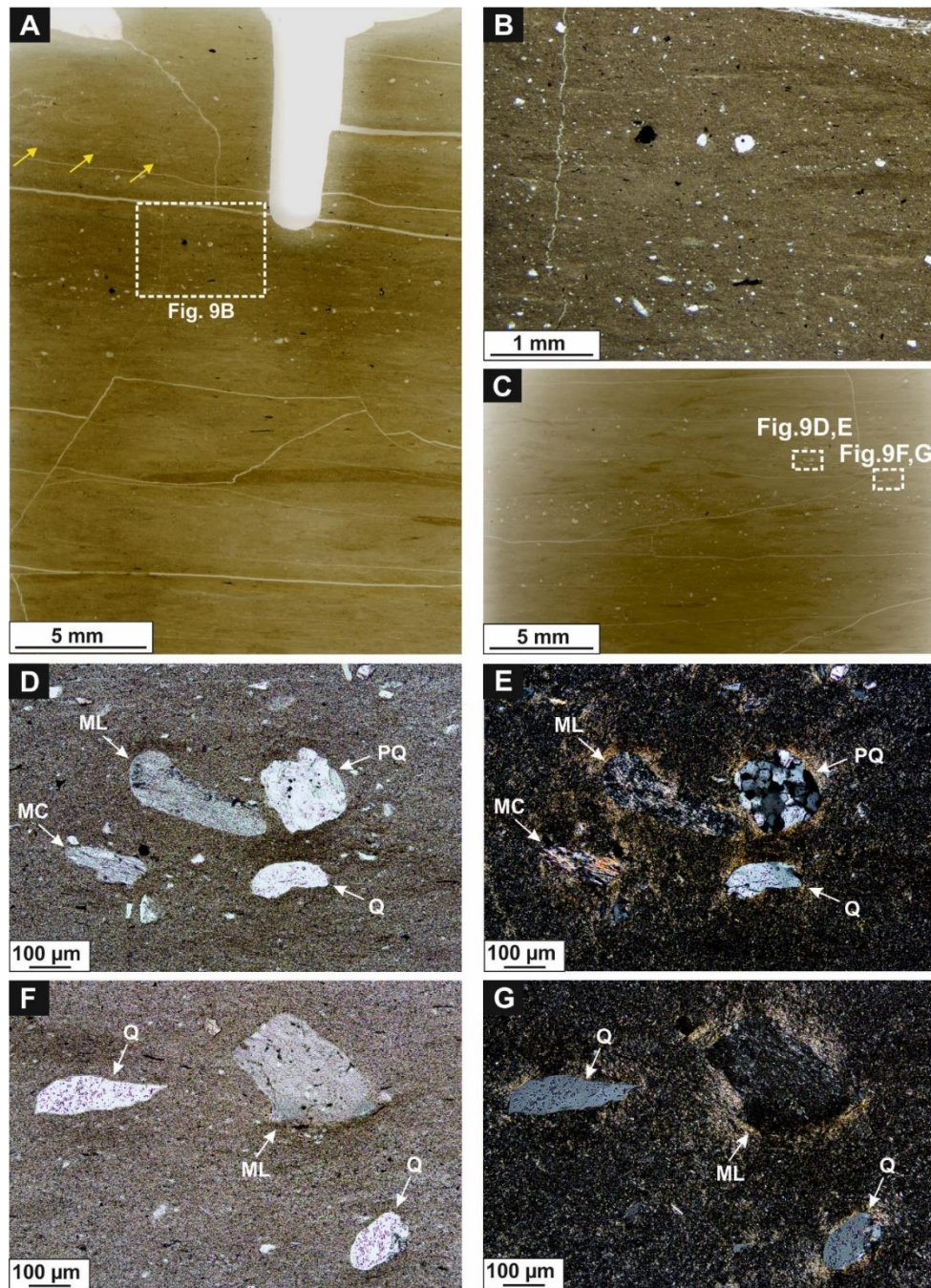
Figure 9: Dispersed outsize particles in Facies 3 (mottled mudstone) from OR01 core. A and C are thin-section scans. B, D, E, F and G are photomicrographs. **A)** Mottled mudstone characterized by a "starry-night" texture (143.75 m). Note the enrichment in outsize particles and the bed base (yellow arrows) in the upper part of the section. **B)** Magnified view of the upper part of the thin section presented in Figure 9A. Note the outsize particles and the poorly sorted texture. **C)** Mottled mudstone characterized by a "starry-night" texture (106.76 m). Note the enrichment in outsize particles in the middle part of the section. Location of Figures 9D, 9E, 9F and 9G shown by white dotted squares. **D)** Plane-polarized light. **E)** Cross-polarized light. **F)** Plane-polarized light. **G)** Cross-polarized light. ML = mudstone lithic, PQ = polycrystalline quartz, Q = quartz, MC = metamorphic clast.
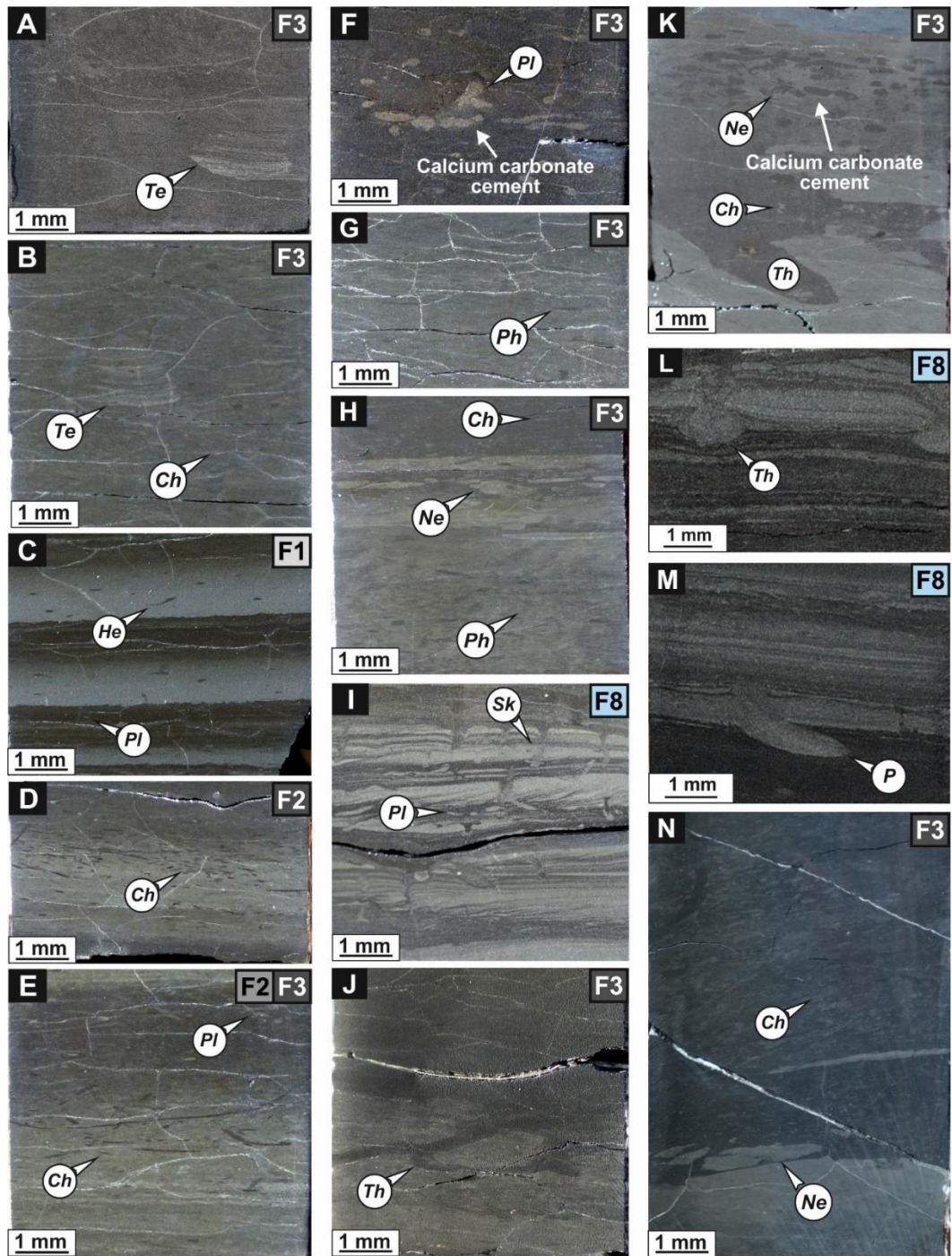
Figure 10: Core photographs of the range of ichnotaxa described in the Skoorsteenberg Formation (from OR01 core). **A)** *Teichichnus* in F3 (394 m). **B)** *Chondrites* and *Teichichnus* in F3 (401.73 m). **C)** *Helminthopsis* and *Planolites* in F1 (258 m). **D)** *Chondrites* in F2 (286.92 m). **E)** *Chondrites* and *Planolites* in F2 and F3 (218.13 m). **F)** *Planolites* in F3 (250.80 m). Burrows are cemented by calcium carbonate. **G)** *Phycosiphon* in F3 (270.30 m). **H)** *Chondrites, Nereites* and *Phycosyphon* in F3 (378.30 m). **I)** *Planolites* and *Skolithos* in F8 (115.90 m). **J)** *Thalassinoides* in F3 (324.30 m). **K)** *Chondrites, Nereites* and *Thalassinoides* in F3 (373.31 m). **L)** *Thalassinoides* in F8 (149.05 m). **M)** *Palaeophycus* in F8 (149.85 m). **N)** *Chondrites* and *Nereites* in F3 (384 m).
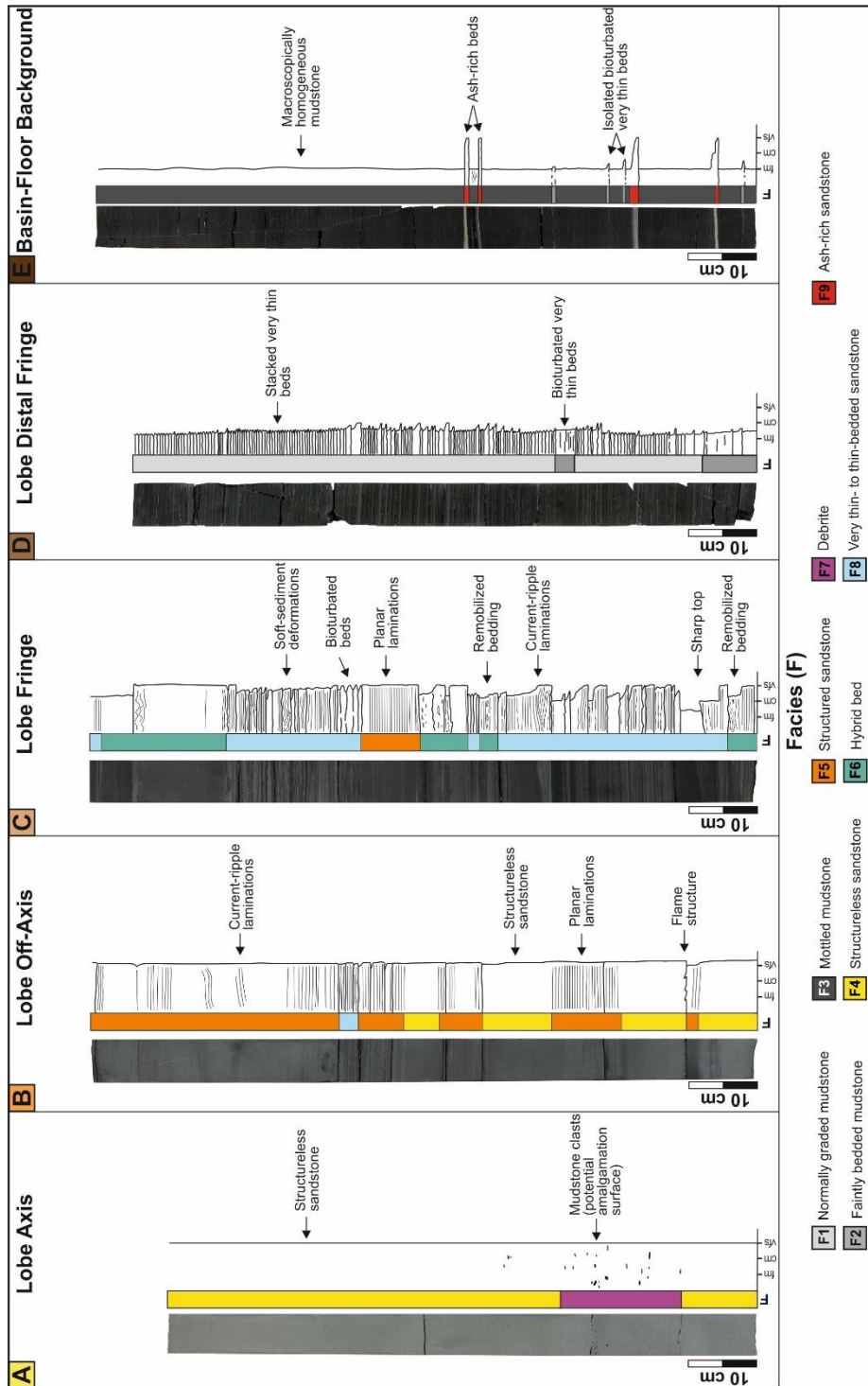
Figure 11: Representative core photographs and sedimentological logs of the different facies associations described in the Skoorsteenberg Formation (from OR01 core). **A)** Lobe axis (from 191.04 m to 190.06 m). **B)** Lobe off-axis (from 199.20 m to 198.30 m). **C)** Lobe fringe (from 136.61 m to 135.64 m). **D)** Lobe distal fringe (from 216.66 m to 215.76 m). **E)** Basin-floor background (from 303.10 m to 302.15 m).
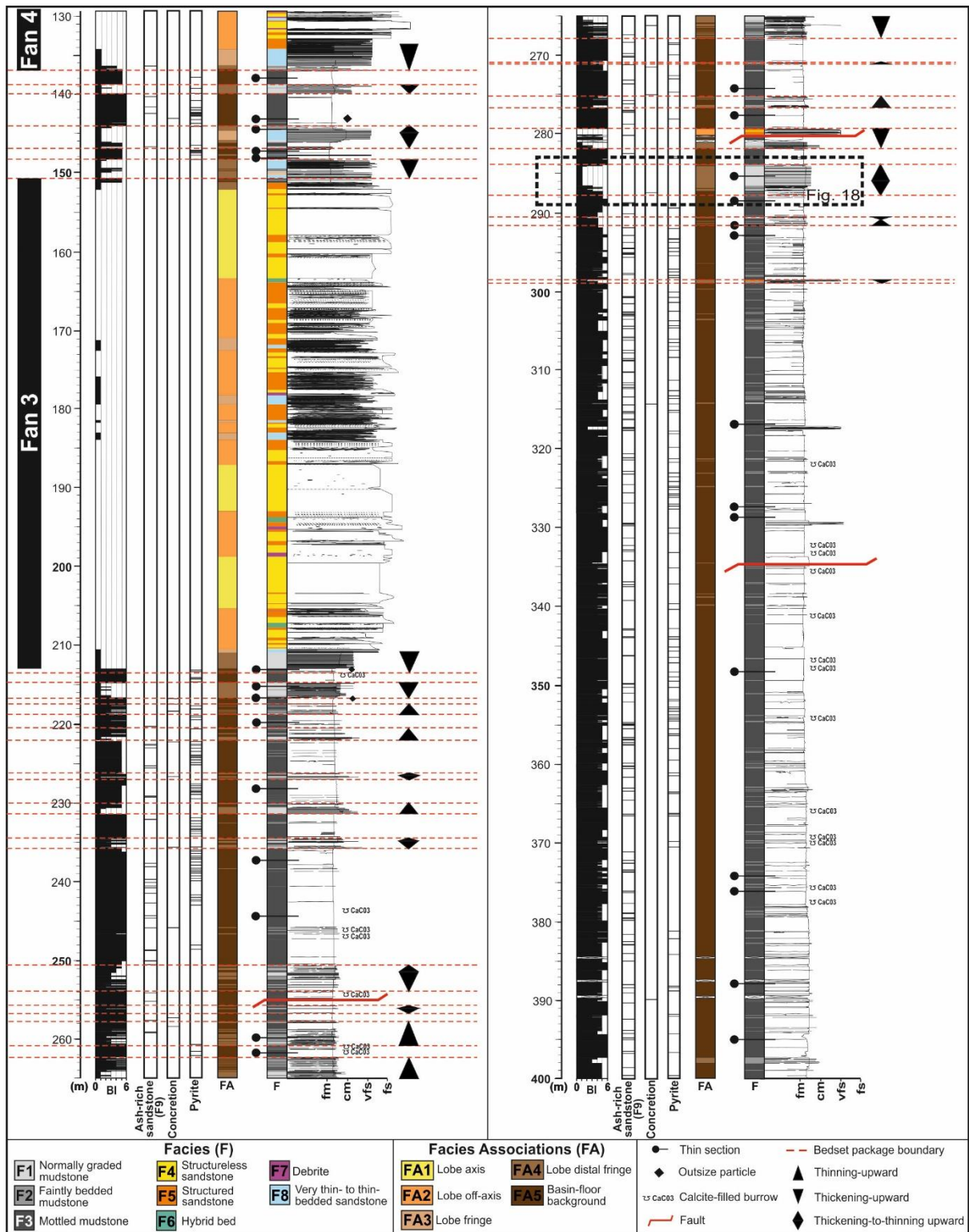
Figure 12: Summarized sedimentological log of the OR01 core (from 400 m up to 130 m), including facies (F), facies associations (FA), bioturbation index (BI), presence of pyrite nodules, carbonate-rich concretions and ash-rich sandstones (F9). Bedset packages are delineated (red dotted lines) with internal stacking pattern. Bioturbation index scale from Taylor and Goldring (1993). fm = fine mudstone; cm = coarse mudstone; vfs = very fine sandstone; fs = fine sandstone.
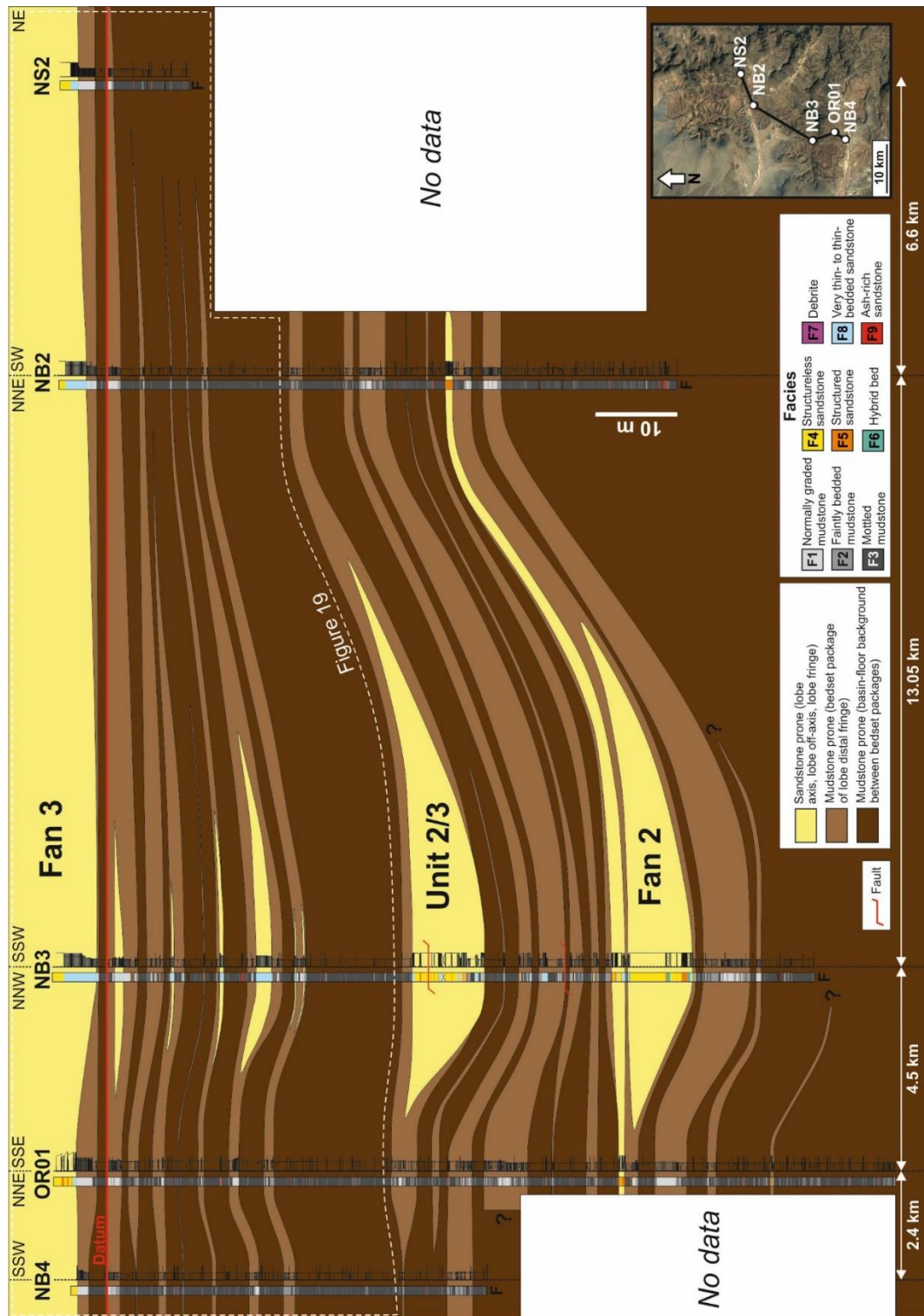
Figure 13: Correlation panel between the different cores (NB4, OR01, NB3, NB2, NS2). The datum for correlation is the base of the laterally continuous package of basin-floor background mudstones (FA 5) directly underlying Fan 3 (red line). Bedset packages of lobe distal fringe deposits have been correlated between the different wells based on the tabularity of basin-floor deposits, and the absence of evidence for significant seafloor topography. Correlation below Unit 2/3 is tentative due to post-depositional faults identify in NB3.
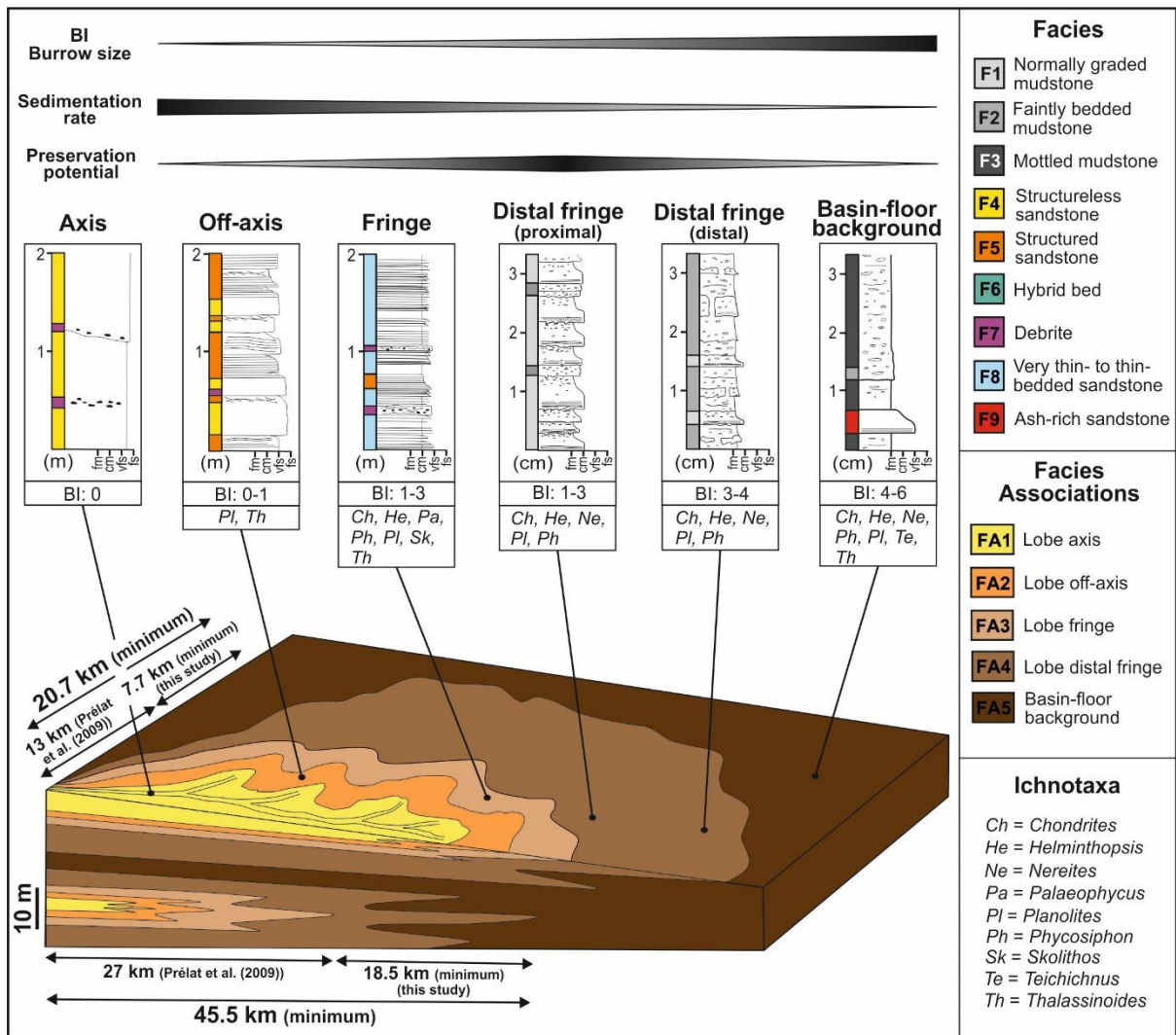
Figure 14: Depositional model of deep-water basin-floor lobes based on the description and interpretation of the Skoorsteenberg Formation. Representative sedimentological logs for each sub-environment are shown, along with facies, facies associations, ichnotaxa and bioturbation index (BI). Note the different vertical scales of the sedimentological logs between the sandstone-prone and mudstone-prone part of the model. Bioturbation index scale from Taylor and Goldring (1993).
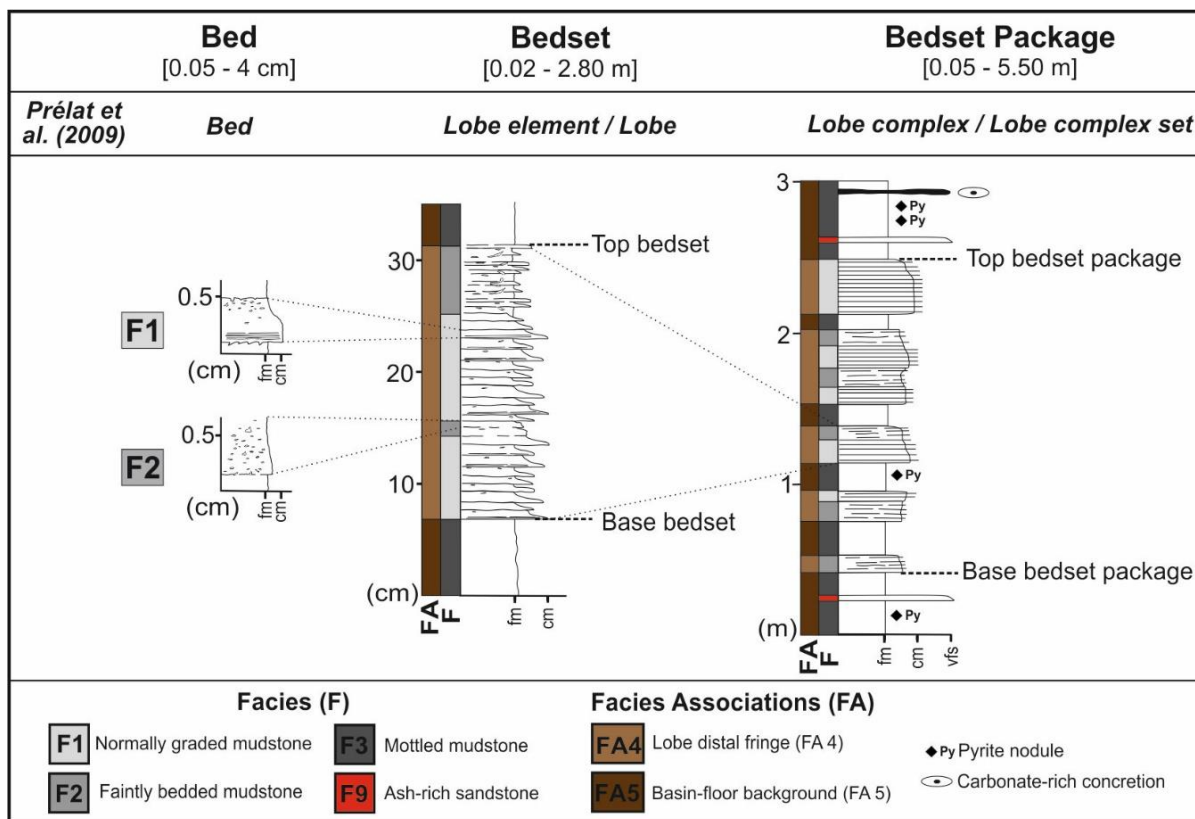
Figure 15: Hierarchical scheme used to stratigraphically subdivide mudstone-prone distal basin-floor fans developed from the distal part of the Skoorsteenberg Formation. The equivalence with the hierarchical scheme developed previously in proximal sandstone-prone basin-floor fans (Prélat et al. 2009) is indicated. Basin-floor background mudstone packages (FA 5) are used as bounding elements of packages of bedded mudstones deposited in lobe distal fringe environments (FA 4). Relatively thin basin-floor background mudstone packages (FA 5; <0.7 m thick) separate genetically-related bedsets of lobe distal fringe deposits (FA 4). Thicker basin-floor background mudstone packages (FA 5; >0.7 m thick), with more common ash-rich sandstones (F9) and carbonate-rich concretions, separate bedset packages of lobe distal fringe deposits (FA 4).
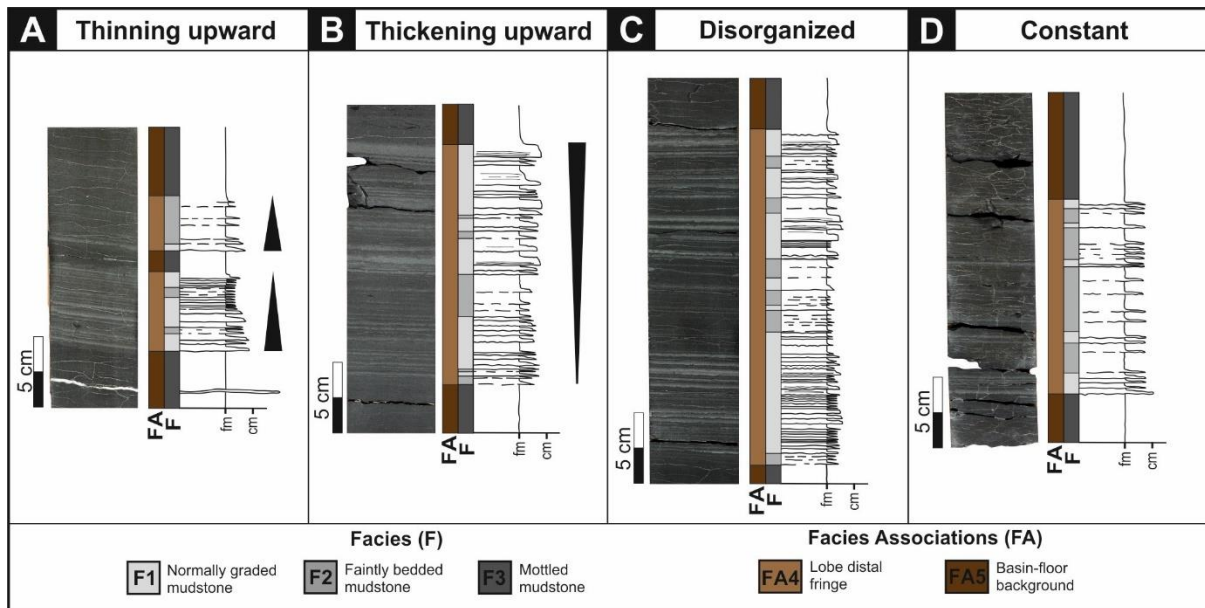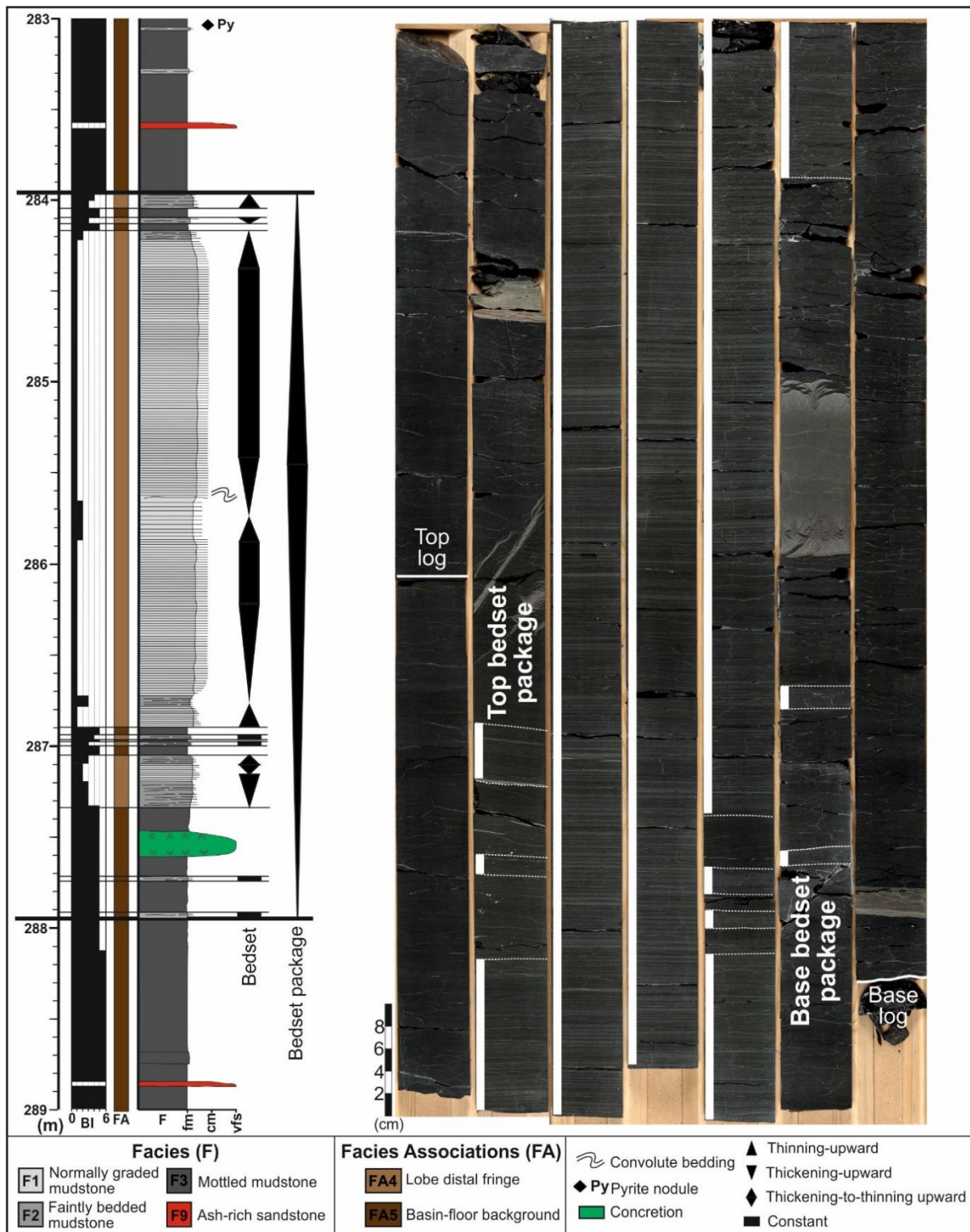
Figure 16: Representative core sections and sedimentological logs of the different bedset stacking patterns of lobe distal fringe deposits (FA 4) observed in the distal part of the Skoorsteenberg Formation (OR01 core). **A)** Thinning upward (from 258.95 to 258.75 m). **B)** Thickening upward (from 147.50 to 147.25 m). **C)** Disorganized (from 260.15 to 259.87 m). **D)** Constant (from 221.25 to 221).
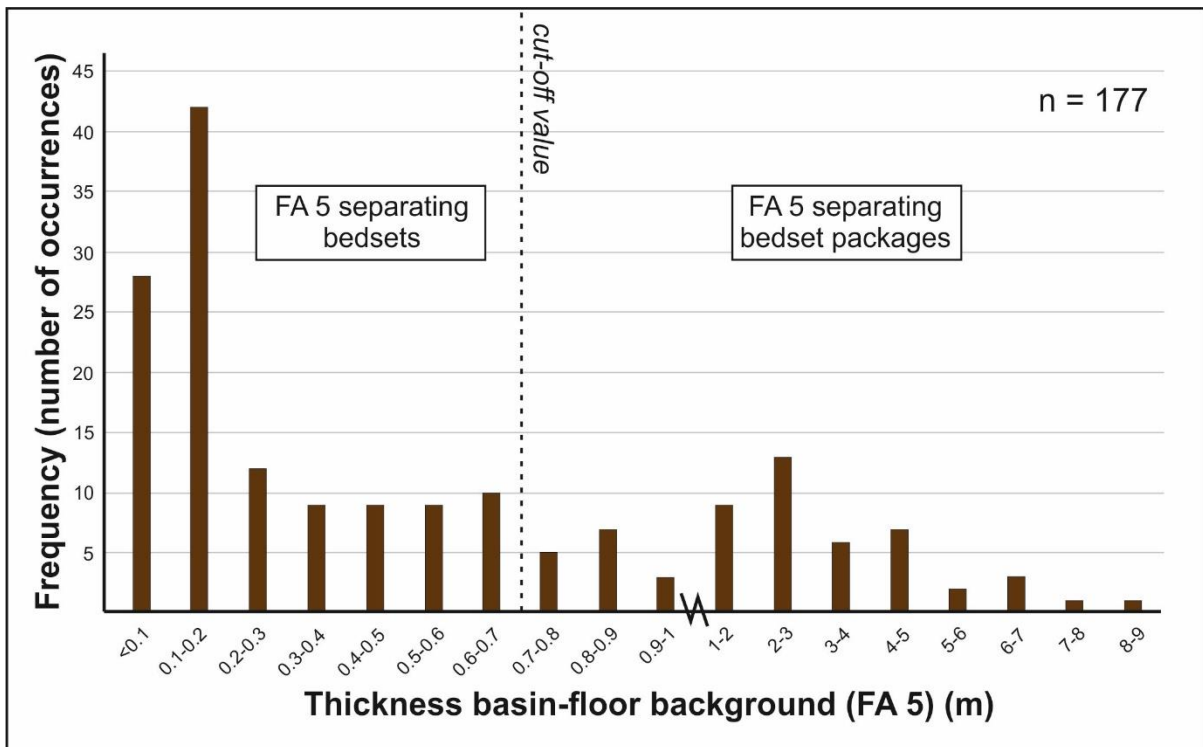
Figure 17: Histogram showing the thicknesses of packages of basin-floor background deposits (FA 5) compiled from the five research boreholes used in this study (OR01, NB2, NB3, NB4 and NS2). Note the horizontal scale change at 1 m. The marked decrease in frequency of FA 5 thicknesses values identified at 0.7 m suggests that a FA 5 thickness of 0.7 m can be used as a cut-off value to differentiate two distinct hierarchical orders within this succession: i) relatively thin packages of basin-floor background deposits (FA 5; <0.7 m thick) separate vertically genetically-related bedsets of lobe distal fringe deposits; ii) relatively thick packages of basin-floor background deposits (FA 5; >0.7 m thick) separate vertically bedset packages of lobe distal fringe deposits.

Figure 18: Representative core section and sedimentological log of the stacking pattern within a bedset package (from 289 m to 283 m; OR01). See stratigraphic position in Figure 12. The bedset package consists of eight bedsets (indicated by the white rectangles in the core picture), and is coarsening- and thickening-upward followed by fining- and thinning-upward. Bioturbation index (BI) scale from Taylor and Goldring (1993).
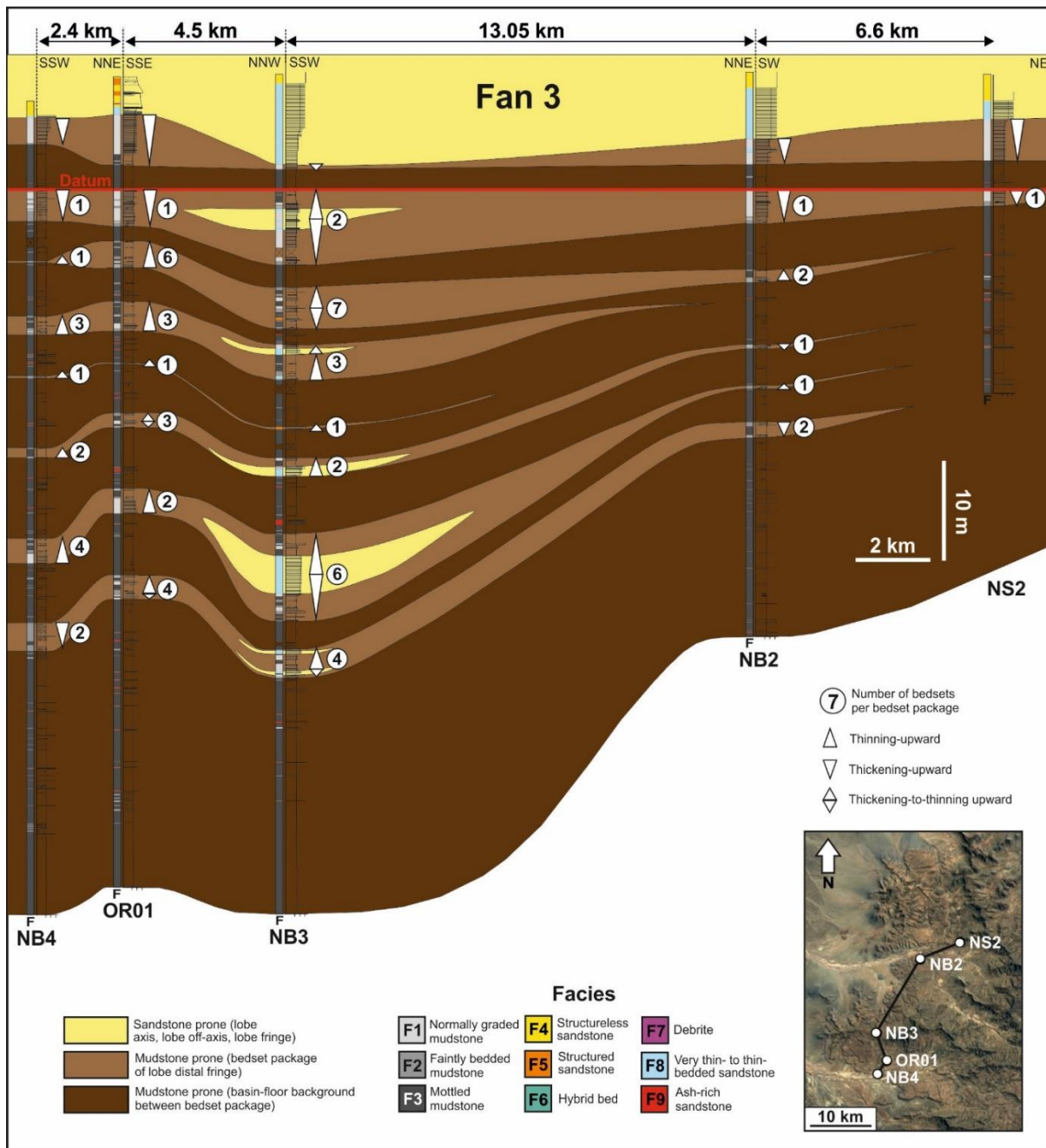
Figure 19: Correlation panel of the bedset packages of lobe distal fringe deposits below Fan 3. The datum for correlation is the base of the laterally continuous package of basin-floor background mudstone directly underlying Fan 3 (red line). The stacking pattern of bedset packages, which represent lobe complexes or lobe complex sets, and the number of constituent bedsets per package (from 1 up to 7), which represent lobe elements and/or lobes, are indicated. Note the lateral and vertical variability of bedset package stacking pattern and number of constituent bedsets.